NAVAL POSTGRADUATE SCHOOL
Monterey, California

THESIS

MEASUREMENT OF SYNCHRONOUS FORCES
AND FLOW NON-UNIFORMITY IN AN AXIAL
COMPRESSOR

by

Alvaro F. Cuellar

December, 1997

Thesis Advisor: K. T. Millsaps, Jr.

Approved for public release; distribution is unlimited.

19980505 033

REPORT DOCUMENTATION PAGE		Form Approved OMB No. 0704-0188

1. AGENCY USE ONLY *(Leave blank)*	2. **REPORT DATE** **December 1997**	3. **REPORT TYPE AND DATES COVERED** **Master's Thesis**

4. TITLE AND SUBTITLE **MEASUREMENT OF SYNCHRONOUS FORCES AND FLOW NON-UNIFORMITY IN AN AXIAL COMPRESSOR**	5. FUNDING NUMBERS
6. AUTHOR(S) Alvaro F. Cuellar	

7. PERFORMING ORGANIZATION NAME(S) AND ADDRESS(ES) Naval Postgraduate School Monterey CA 93943-5000	8. PERFORMING ORGANIZATION REPORT NUMBER
9. SPONSORING/MONITORING AGENCY NAME(S) AND ADDRESS(ES)	10. SPONSORING/MONITORING AGENCY REPORT NUMBER

11. SUPPLEMENTARY NOTES The views expressed in this thesis are those of the author and do not reflect the official policy or position of the Department of Defense or the U.S. Government.

12a. DISTRIBUTION/AVAILABILITY STATEMENT Approved for public release; distribution is unlimited.	12b. DISTRIBUTION CODE

13. ABSTRACT *(maximum 200 words)* Time resolved pressure measurements on a compressor case were acquired for several uniform and non-uniform tip clearances. High frequency response pressure transducers were placed at several axial locations near the second stage axial rotor on the outer casing of an Allison C-250 compressor. Data were acquired at several fixed time intervals. The amplitude of the blade-to-blade variations and once per revolution static pressure distributions on the case were recorded for an "as is" compressor. The synchronous forces due to possible imperfections were determined using a high hub-tip ratio assumption.

14. SUBJECT TERMS: Turbomachinery, Rotor dynamics	15. NUMBER OF PAGES **89**
	16. PRICE CODE

17. SECURITY CLASSIFICATION OF REPORT Unclassified	18. SECURITY CLASSIFICATION OF THIS PAGE Unclassified	19. SECURITY CLASSIFICATION OF ABSTRACT Unclassified	20. LIMITATION OF ABSTRACT UL

i

MEASUREMENT OF SYNCHRONOUS FORCES AND FLOW NON-UNIFORMITY IN AN AXIAL COMPRESSOR

Alvaro F. Cuellar
Lieutenant, United States Navy
B.S.M.E., Virginia Military Institute, 1988

Submitted in partial fulfillment of the
requirements for the degree of

MASTER OF SCIENCE IN MECHANICAL ENGINEERING

from the
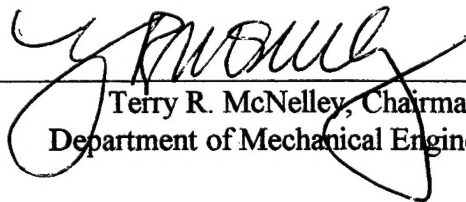
NAVAL POSTGRADUATE SCHOOL
December, 1997

Author: _____
Alvaro F. Cuellar

Approved by: _____
Knox T. Millsaps, Jr., Thesis Advisor

_____
Terry R. McNelley, Chairman
Department of Mechanical Engineering

iii

ABSTRACT

Time resolved pressure measurements on a compressor case were acquired for several uniform and non-uniform tip clearances. High frequency response pressure transducers were placed at several axial locations near the second stage axial rotor on the outer casing of an Allison C-250 compressor. Data were acquired at several fixed time intervals. The amplitude of the blade-to-blade variations and once per revolution static pressure distributions on the case were recorded for an "as is" compressor. The synchronous forces due to possible imperfections were determined using a high hub-tip ratio assumption.

TABLE OF CONTENTS

ACKNOWLEDGMENT

x

I. INTRODUCTION

A. SYNCHRONOUS FLUID FORCES ON ROTORS

Gas turbine rotor-bearing systems, as well as, other high speed turbomachines, experience lateral synchronous vibration. The source driving of these vibrations is generally considered to be inertial forces from unbalanced masses. To reduce the magnitude of these vibrations, machines are typically balanced, as described by Muster and Stadelbauer [1].

However, other synchronous forces are possible, such as electromagnetic forces in motors and generators and fluid forces in turbomachines, as described by Den Hartog [2]. In particular, a spinning rotor that contains first harmonic deviations from perfect symmetry may generate radial and tangential forces. Higher order harmonics will not generate net forces, if sufficiently small perturbations are considered on the rotor. Such geometrical imperfections are due to standard machining tolerances and/or service wear. Recent experience with several high power density rotors suggest that spools that are well balanced in the absence of fluid forces may encounter synchronous vibrations in excess of those that can rationally be attributed to the inertial forces. One possible cause is the fluid forces due to geometric asymmetry. These forces will have a magnitude and phase which are stationary in the rotating frame, at a given flow condition. For constant speed machines, it is likely that dynamic trim balancing can counteract these fluid forces. However, in machines with widely varying flow conditions, this may not be the case. This is due to the different magnitude and phase scaling character of the rotor inertial forces and the fluid forces.

Asymmetries in compressors, turbines and sealing elements can create non-uniform flows which in turn generate once per revolution forces on a rotor. Seals, such as labyrinths, can have non-uniform gaps, as well as, local imperfections in the sealing knives which can lead to a rotating non-uniform pressure inside the glands. Williston [3] and Millsaps and Williston [4] have developed a lumped parameter model for synchronous seal

1

forces. The model predicts that the fluid induced forces can be of the same order of magnitude as the maximum allowable inertial forces with high grade balance tolerances for some conditions.

Turbomachines have a variety of rotating imperfections, such as variations in blade shape (camber and thickness distribution), stagger angle, tip clearance, etc. Presumably for small deviations, each can be investigated separately to determine the overall effect. An imperfections that is likely to exist in a real compressor is a variation in the tip clearance around the rotor. The nominal tip clearance is typically 0.001 inch per inch of rotor radius. This allows for relative growth of the rotor and casing (both inertial and thermal), plus misalignment and vibration. Very small absolute variations in the rotor's circularity can lead to significant variations in gap around the casing in percentage terms. Therefore, it seems likely that this is the dominant non-uniformity that will exist in turbomachines. A non-circular casing will lead to a stationary redistribution of flow and hence only a static force on the rotor. Synchronous forces generated by a non-uniform rotating tip clearance in a compressor are the subject of this work.

B.   BACKGROUND AND STATE OF THE ART

To the best knowledge of the author there is no previous work which examines the synchronous radial forces on a compressor or turbine rotor due to a rotating tip imperfection. However, there has been work in several closely related topics which are relevant to this investigation.

In particular, the impact of uniform tip clearance on compressor efficiency and stall margin has been extensively investigated by Rains [5] and others [6, 7, 8, 9, 10, 11, 12]. As a rule of thumb the efficiency degrades about 1.5% per 1% of tip clearance (based on blade height) and the stall margin degrades about 3% per 1% increase in tip gap.

Horlock and Greitzer [13] presented an actuator disk analysis of several non-uniform tip gap conditions in a compressor, including a rotating non-uniform tip clearance. They concluded that a non-uniform rotating gap produces nearly twice the velocity

2

perturbation as a stationary one under similar conditions. This analysis was done for high hub-tip ratio machines and hence neglects radial variations (i.e. static pressure perturbations at the tip are assumed to penetrate to the hub).

Graf [14] has used the actuator disc model to predict the stability of compressors due to a non-uniform tip clearance. He predicted that the stability is degraded more than would be expected based on the average gap.

A closely related problem of a rotating non-uniform rotor with variable blade height is the problem of a "perfect" rotor whirling in a "perfect" casing. The flow physics of the two phenomena are quite similar. In fact, if the whirl speed is taken to the same as the rotor spin speed, the principle difference between these two problems is that for the spinning non-uniform tip clearance, there is no perturbation in the hub geometry as there would be with a synchronous whirling rotor. Hence, a review of the literature for this similar problem will be given.

Thomas [15] and Alford [16] have proposed models to predict cross forces on a circular turbine rotor in a circular casing with a static parallel offset. This deflection creates a static (non-rotating) first harmonic distribution of tip clearance around the annulus. Both models assume that the upstream and downstream flow are uniform. The variation in efficiency creates higher tangential blade forces at the part of the annulus with tight clearance than at the wider clearance, where the blade tip is unloaded. The integrated effect from all the blades is to generate a positive (in the same sense as the direction of rotation) cross stiffness for a turbine. Urlichs [17], Wohlrab [18], Vance [19], and Loose [20] measured these forces and found them to be in the forward direction as predicted by the simple theory. Song and Martinez [21, 22] have extended the theory to relax the uniform inlet and exit conditions by applying the Horlock-Greitzer model. They also measured the forces on a shrouded and unshrouded turbine. All measurements on turbines presented in the open literature have shown that the cross forces are in the forward direction as predicted by theory.

The situation with respect to predicting tangential forces due to an offset compressor rotor is more controversial. Colding-Jorgenson [23] used an actuator disk

model to predict that the forces should promote forward whirl for all reasonable flow coefficients. Only at flow coefficients well below those associated with stall does the Thomas-Alford coefficient change signs to promote backward whirl. Ehrich [24] presented a parallel compressor model, based on data from several uniform clearance compressors, to predict that the cross forces should be in the same direction as the spin at high flow coefficients and cross over to backward whirl promoting forces at lower flow coefficients. Ehrich predicted that typical compressors will have backward whirl producing forces at a stalling mass flow.

Measurements of tangential forces and pressure distributions due to a statically offset circular compressor rotor in a circular casing have been reported by Vance and Laudadio [25] and Lintang, Qihan, et al. [26]. Vance et al measured cross forces on a low speed fan with large tip gaps. Litang et al measured casing static pressures and cross forces in a compressor rotor. The flow coefficients at which these measurements were taken were not reported by either. This quantity is necessary to correlate experimental results with theory.

In summary, no work has been reported on the synchronous radial and tangential forces produced by a non-uniform rotating tip clearance. For the similar problem of an offset or whirling compressor rotor there is considerable uncertainty as to the magnitude these forces and the phase of the force relative to the minimum gap.

C.   PURPOSE AND SCOPE OF WORK

Due to the contradicting results from the actuator disk and parallel compressor models for the Alford-Thomas forces, it is doubtful that such simple analyses can provide a clear answer to the related problem of forces generated by a non-uniform rotor. Therefore, a need exists to obtain direct experimental data on the magnitude and phase of the forces on a compressor due to a non-perfect rotor.

This thesis represents a contribution to the effort to measure and predict the flow fields and synchronous forces generated by imperfect compressor rotors. Specifically, an

4

experimental program was conducted to measure the existing spatial and temporal non-uniformity of static pressure on the case of a compressor over a rotor in an "as is" condition in several locations. "As is" refers to no mechanical changes to the compressor and turbine since the last depot level overhaul of the gas turbine engine.

After these reference (baseline) measurements are completed, the rotor will be ground to a near perfect circularity and similar casing static pressure measurements made. Finally, a first harmonic imperfection in the rotor tip length will be imposed by machining a first harmonic distribution and measurements made. With these measurements, it is believed that the forces due to tip clearance imperfections can be extracted.

Information from the "as is" rotor will be used to guide future efforts. Specifically, information on how the non-uniform gaps influence the near-field boundary conditions is being sought, as well as, good locations for transducer placement, etc. Therefore, information obtained from these measurements will be valuable in the program in the future.

The objectives of this thesis are to instrument a single stage of an axial compressor for time resolved casing static pressure measurements. The characteristics of these signals are sought. Of particular interest in the measurements is the presence or absence of power in the signal at rotor speed. Using the methodology planned to extract synchronous forces depends on being able to extract the component of the signal at rotor speed from a complex signal which has dominant energy at blade passing. Demonstrating the ability to acquire and process these signals is a necessary step.

D.   THESIS OUTLINE

This document is organized in the following manner:
Chapter II provides the experimental set-up and hardware used in testing the gas turbine engine. Chapter III describes the data acquisition hardware and system interface used in this experiment. Chapter IV covers the analyses of data and interpretation of measured

values. Chapter V provides the concluding remarks and recommendations for further research in this area.

II. EXPERIMENTAL SETUP

A.   FACILITY DESCRIPTION

This experimental investigation was conducted in the Marine Propulsion Laboratory at the Naval Postgraduate School in Monterey, CA. A gas turbine test cell houses and supports the operation of the engine which is mounted on a water brake dynamometer test stand with a *SF-901 Model* operating control system manufactured by *Superflow Corporation*, Colorado Springs, CO. The facility allows for computer control of the engine, specifically throttle and load control. Compressor speed (N1), gas generator speed (N2) and output shaft speed are monitored along with other operating parameters using the *Superflow Data Acquisition System*. Eckerle[29] and Hass[30] outline specific engine operation and *Superflow* data acquisition procedures used in this experiment.

B.   GAS TURBINE ENGINE DESCRIPTION

The gas turbine engine used was an Allison Gas Turbine designated as T63-A-700 (Military version) manufactured by Allison Division, General Motors Corporation, Indianapolis, IN (Figure 2.1). The engine has a design output power of 317 HP. The 2 stage, free power turbine speed at this output power is 35,000 RPM, coupled to a reduction gear, with a speed ratio of 5.833:1, allowing the output shaft to rotate at 6,000 RPM. The U.S Army uses this engine as the main drive for the *Bell Inc.*, Jet Ranger (OH-58) reconnaissance helicopter. The gas turbine engine leading particulars are given in Table 2.1.

C.   AXIAL COMPRESSOR DESCRIPTION

The compressor is an axi-centrifugal type with six axial stages followed by a single centrifugal stage on a single spool. Air enters the compressor front frame through a set of stationary inlet guide vanes to induces swirl to the flow, then air enters stages 1 through 6, consisting of one rotor and one stator row per stage. The individual stage pressure ratios

7

are listed in Table 2.2. The pressure ratio for the axial compressor (π_{axi}) is 2.6 and for the centrifugal compressor (π_{cent}) is 2.2, thus, an overall design pressure ratio (π_c) of 5.72:1.

An ablative, thermal plastic setting is centrifugally cast onto the lining of the two compressor split halves to minimize the rotor tip clearance, hence improving compressor efficiency. The nominal tip clearance for this compressor is near zero. That is, the gap between the rotating blade tips and the inner casing have a nearly immeasurable tolerance.

The compressor speed for inlet conditions at Standard Pressure and Temperature (P = 29.92" Hg and T = 59° F) is 51,120 RPM which corresponds to an entering mass flow rate equal to 3.13 LBM/SEC and an axial Mach Number equal to 0.43 [31, 32].

The blading material used for all stages is a precipitation hardened, cast, stainless steel. The rotor and stator blading is a double circular arc (DCA) [32] cantilevered blade construction with the blades per stage and rotor blade characteristics listed in Table 2.2.

The 2nd row of the axial flow compressor was chosen for measurement as discussed in Chapter II, section E.

D.   INSTRUMENTATION RING DESIGN AND INSTALLATION

It was necessary to determine a method for securing the flush mounted pressure transducers at the proper locations over the second stage of the rotor. These transducers had to be held radially inward with tolerances of about 0.005" and the penetration through the case had to be well sealed to prevent leakage. Even the slightest penetration of the transducer into the case could allow the high speed rotor to scrape off the tip of the transducer. The existing case wall was too thin for direct mounting. Therefore, an auxiliary mounting ring had to be designed to hold the transducers.

This instrumentation ring which consist of two halves that bolt on with the compressor split casing is shown in Figures 2.3a and 2.3b. This ring was designed to fit around the existing case with a tight clearance fit so as not to distort the casing and therefore not to alter the tip clearances inside. The instrumentation ring has tapped 10-32 UNF (fine threads) through threaded holes for the insertion of the pressure transducers.

8

Also a 1/4-28 hole was drilled and tapped to allow the placement of an eddy current proximeter. Mating plug bolts were manufactured for all holes to seal the ports that are not in use. The compressor case had plain through drilled clearance holes for all transducers. The ring was made of Aluminum at the NPS M.E. machine shop and the dimensions and tolerances are given in Appendix A.

E.   SELECTION OF TRANSDUCER LOCATIONS

The pressure transducers were placed over the rotor blade at the $1/3^{rd}$ and $2/3^{rd}$ axial chord locations on the compressor casing also before the rotor inlet and after the outlet of the 2nd row blading was instrumented. These locations are shown in Figure 2.4. These locations were selected based on:

1.   The axial chord locations that will provide an accurate representation of the flow non-uniformity that might occur away from the leading edge and trailing edge of the airfoil profile [8, 31].

2.   Blades at the 2nd stage are not cropped for balancing or prevention of resonant blade frequencies like stages 3 and 6.

3.   Minimal external interference to accommodate the transducer and instrumentation ring

4.   The air temperature at the 2nd stage is relatively low. This minimized the problem of thermal compensation for the pressure transducers.

For this experiment, the only pressure measurements obtained were at the $1/3^{rd}$ and $2/3^{rd}$ location that characterized the flow patterns for a blade-to-blade passage.

F. AXIAL COMPRESSOR INSTRUMENTATION

The instrumentation of the compressor included 4 (four) *Kulite Semiconductor* transducer (Figure 2.4), which were flush mounted to the casing to measure time resolved casing static pressures at various locations. Two miniature, *United Sensor Technology*, combination Kiel and temperature sensing devices (Figure 2.5), were used to measure the compressor outlet total pressure and total temperature. Haas [30] describes the particulars of this probe in detail.

1. Pressure Transducers

The *Kulite Semiconductor* pressure transducers used in this experiment were the Model XCS-190D which provided a frequency response rated to 100 kHz with an operating range of 5 psid. Each transducer had a back pressure port that was referenced to the average pressure before the stage by a manifold fed from the inlet side of the 2nd rotor stage.

Two pairs of *Kulite* transducers were located radially, 180° apart to measure the pressure waveform induced by the passing blades. These pressures in the casing were denoted by P_{1w} and P_{2w} on the upper compressor half (Figure 2.3a) and P_{3w} and P_{4w} on the lower compressor half (Figure 2.3b) and channel assignments were as follows:

P_{1w} = Channel 1 (1/3rd Axial Chord - top half of the compressor)

P_{2w} = Channel 2 (2/3rd Axial Chord - top half of the compressor)

P_{3w} = Channel 3 (1/3rd Axial Chord - bottom of the compressor)

P_{4w} = Channel 4 (2/3 Axial Chord - bottom of the compressor)

This channel assignment will be used to discuss the results in Chapter IV.

2. Transducer-Conditioning Amplifier

The signal amplifier, *Ectron Corporation Model 563H* (Figure 2.6) was used to condition the raw signals from the *Kulite* transducers. All pressure transducers were excited to +15 volts. The filters were set to wideband and a gain level of 20 was used.

3. Combination Kiel and Temperature Probe

The combination probe in Figure 2.6 was manufactured by *United Sensor Corporation* in Amherst, New Hampshire, that measured the compressor discharge total (stagnation) pressure (P_{T2}) and a high-temperature Chromal-Constantan K-type thermocouple that measured the compressor discharge total temperature (T_{T2}). Two of these measuring devices were fitted on the scroll diffuser of the compressor casing, thus able to measure an average of the compressor discharge condition (P_{T2} and T_{T2}).

4. Additional Steady State Instrumentation

The remaining set of parameters measured were 8 pressure signals and 57 thermocouples located throughout the engine. These values are sufficient pressure to measure and evaluate the thermodynamic cycle. For particulars, see Haas [30].

5. Eddy Current Proximeter

A Bently Nevada eddy current Proximity Transducer system was installed to trigger data acquisition and clock the sampling rate. The installation of this proximeter will enhance the data acquisition process lending itself for phase lock and data acquisition and ensemble averaging. This transducer system was not used in this experiment due to the lack of frequency response of the proximeter system at operational speeds.

11

G.   MASS FLOW INSTRUMENTATION

1.   Turbine and Bellmouth Mass Flow Measurements

To measure the air mass flow into the compressor 2 separate systems were used. The first system was a turbine flow meter installed on the air inlet box and measured by the *Super Flow Dynamometer Data Acquisition*. The second system was a calibrated bellmouth. System calibrated bellmouth, two components were installed and one system was in-place. The two installed components measured the differential pressure across the bellmouth and the in-place system used turbine flow meters to calculate the mass flow entering bellmouth. Each system will be discussed individually.

2.   Differential Pressure Transducer for Inlet Flow Conditions

A small stagnation probe was installed at the centerline axis of the compressor inlet (diameter = 0.125 in) to measure the inlet total pressure (P_{T1}). Around the minimum throat area of the bellmouth, three taps (diameter = 0.025 in) on a common circular manifold, measured the average inlet static pressure (P_S). Using these two pressures, an *MKS Instruments Inc.*-Type 698 differential high-accuracy pressure transducer (range = 20 psid) in conjunction with the *MKS Instruments Inc.* Signal Conditioner Type 270B was used to measure the difference between the total and static pressures ($P_{T1} - P_S$).

See Appendix B for further explanation of the mass flow calculations using these measured parameters.

3.   Installed Turbine Flow Meter for Inlet Conditions

The installed turbine flow meters measured and displayed an air flow quantity in Standard Cubic Feet per Minute (SCFM) which is the calculated value of air flow if

atmospheric conditions were $P_{std} = 29.92"Hg$, $T_{std} = 60^oF$ and no moisture in the air. The *Superflow Operating Manual* states that T_{std} is 60^oF, while Standards in the ASHREA Handbook state $T_{std} = 68 \, ^oF$. See Appendix B for further explanation of the mass flow calculations.
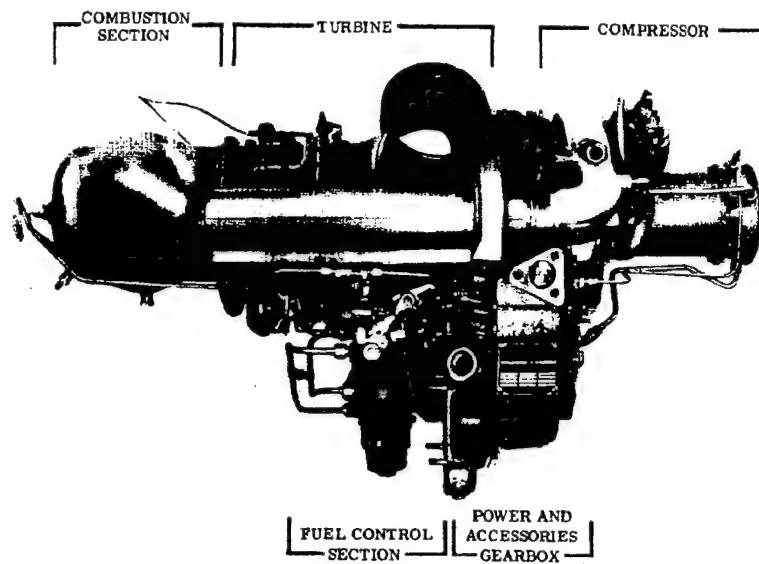
Figure 2.1 T63-A-700 / C250-18 Allision Gas Turbine Engine. Ref [31].

Figure 2.2 Internal view of flush mounted *Kulite* on the bottom compressor half.
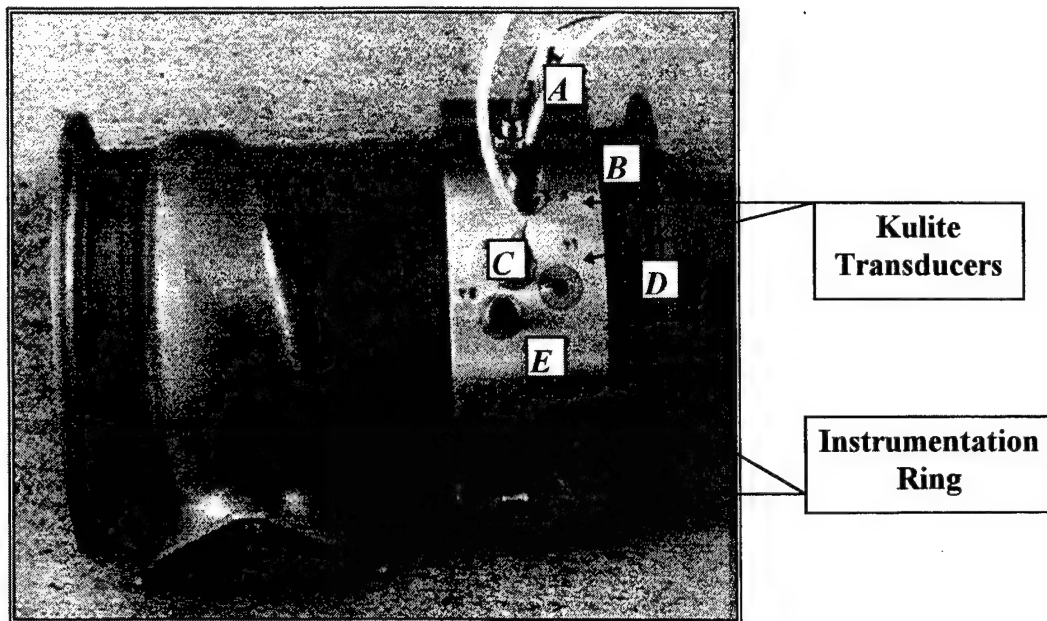
Figure 2.3a Upper compressor casing half Location *A* designates the location of the proximeter, *B* designates the 1/3rd axial chord location for Channel 3, *C* designates the 2/3rd axial chord location for Channel 4, *D* designates the inlet location of the 2nd stage rotor blades, *E* designates the outlet location for the 2nd stage rotor blades.
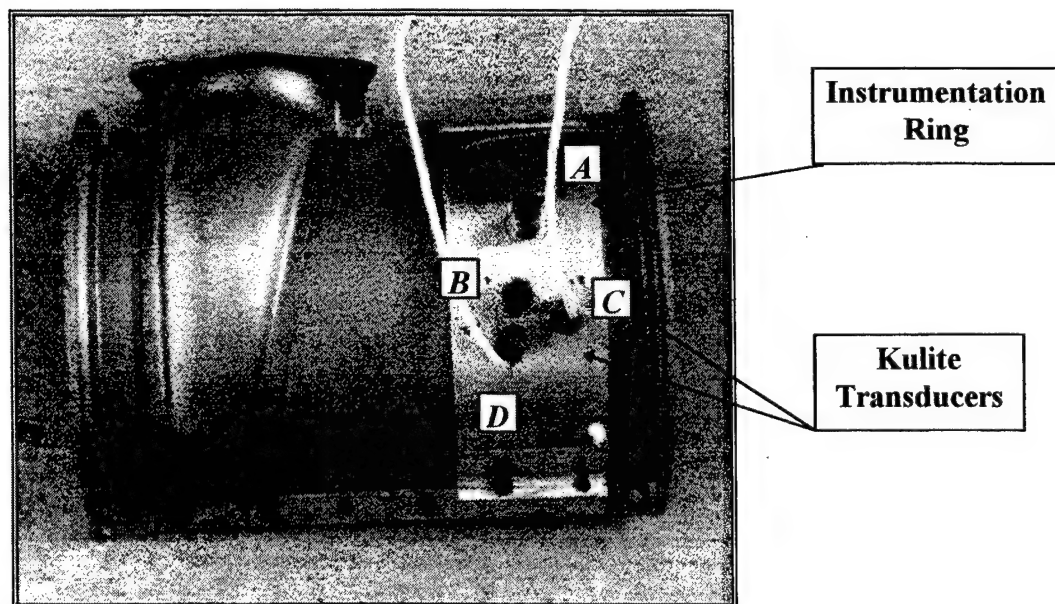
Figure 2.3b Lower compressor casing half (Location *A* designates the 1/3rd axial chord location for Channel 3, *B* designates the 2/3rd axial chord location for Channel 4, *C* designates the inlet location of the 2nd stage rotor blades, *D* designates the outlet location for the 2nd stage rotor blades.

15
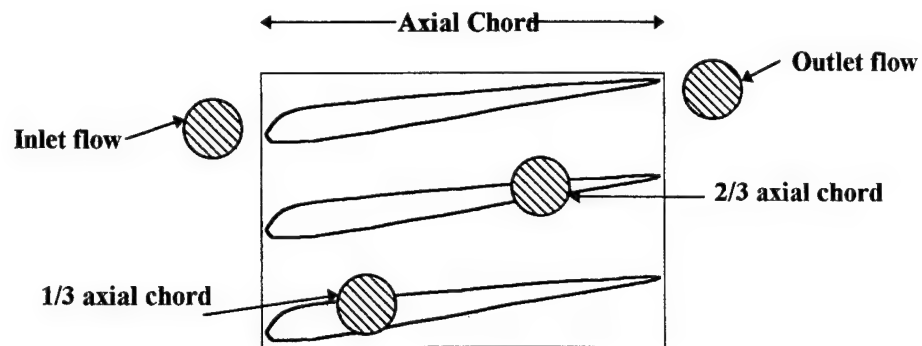
Figure2.4 Schematic Drawing of Transducer location.
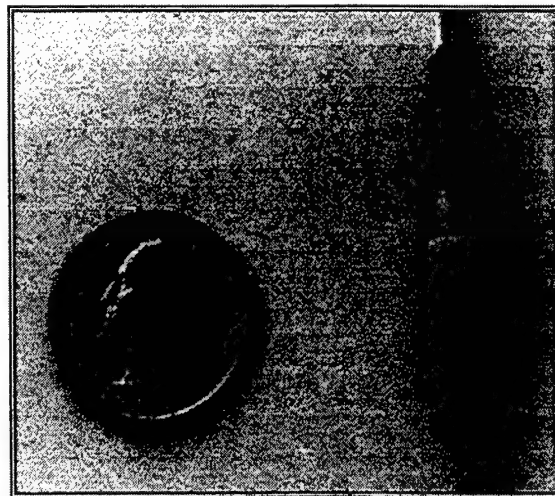
Figure 2.5 XCS-190D Kulite pressure transducer.
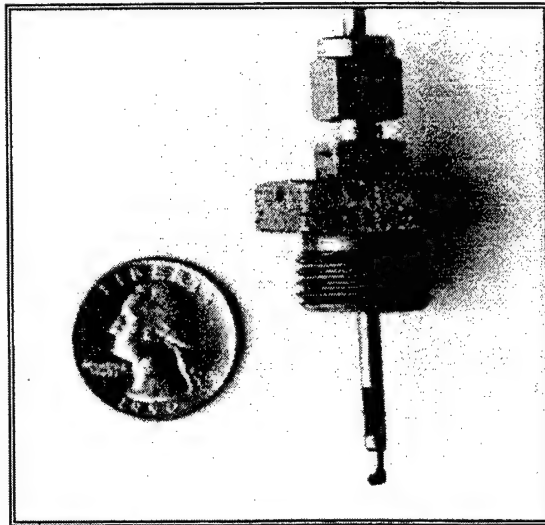
Figure 2.6 Combination pressure and temperature sensor [Ref 30].
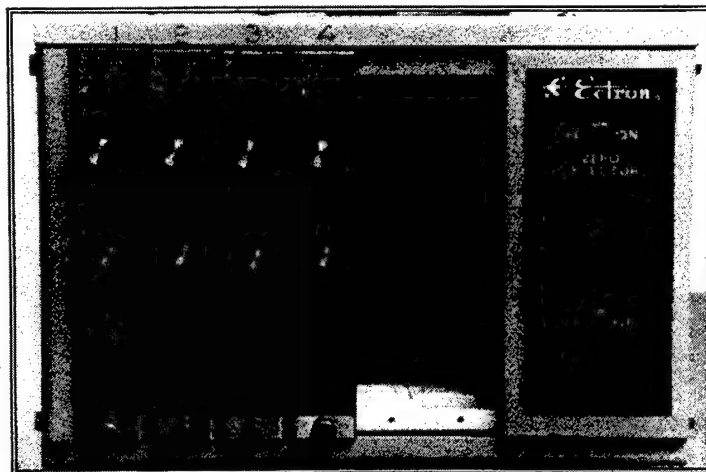
Figure 2.7 Ectron Transducer-Conditioning Amplifier.

Table 2.1 Gas Turbine Engine Leading Parameters [Ref 31].

Dimensions:	Length	40.4 inches
	Height	22.5 inches
	Width	19.0 inches

Engine weight (dry):   138.5 LB

Maximum oil consumption: 0.05 GAL/hr

Lubricating oil specifications: Primary MIL-L-23699
Secondary MIL-L-7808

Oil pressure limits:
    97% N_1 speed and above   110-130 psig
    78%-97% N_1 speed   90-130 psig
    Below 78% N_1 speed   50 psig (minimum)

Oil inlet temperature: Maximum: 225^0 F
Desired operating range: $140\text{-}225^0$ F

Fuel specifications:
    Primary   MIL-L-5625 (JP 4)
    Alternate   Diesel Fuel #2, JP-5, JP-8, JET-A, JETA-1

Design power output:
    Maximum Power (zero air speed @ STP)   317 HP
    Ram Power rating (275 KTS @ STP)   335 HP

Design speeds:
    Gas Generator (N_1)   51,120 RPM @ 100%
    Power Turbine (N_2)   35,000 RPM @ 100%
    Power output shaft   6,000 RPM @ 100%

Overspeed limits:
Gas Generator (N_1)
    Maximum continuous   104% (53,164 RPM)
    Maximum overspeed   105% (53,676 RPM)

Maximum measured gas temperature: $1,380^o$ F (Power Turbine inlet temp.)
$1,510\,^o$ F (Gas Generator inlet temp.)

Maximum output shaft torque:
    Transient (less than 10 seconds)   320 LB-FT
    Takeoff (less than 5 seconds)   293 LB-FT
    Maximum continuous   249 LB-FT

Table 2.2 Individual Stage Characteristics for the Axial Compressor [Ref 31].

	1st Stage	2nd Stage	3rd Stage	4th Stage	5th Stage	6th Stage
Pressure Ratio (π_{1-6})	1.130	1.165	1.179	1.193	1.195	1.188
Average Inlet Total Pressure [psi]	14.54	16.43	19.16	22.58	26.94	32.19
Average Inlet Total Temperature [°R]	519.0	539.7	567.3	599.2	635.2	674.2
Average Inlet Axial Velocity [ft/sec]	500.0	526.0	547.0	554.9	554.1	543.7
Rotor Aspect Ratio	2.17	1.93	1.67	1.47	1.34	1.24
Rotor Hub/Tip Ratio	0.356	0.479	0.570	0.638	0.689	0.727
Rotor Blade Chord [in]	0.605	0.554	0.534	0.510	0.483	0.456
Rotor Blade Camber Angle (midspan) [°]	18.4	24.7	26.7	27.4	28.0	28.1
Rotor Blade Radius (midspan) [in]	1.466	1.598	1.697	1.770	1.825	1.867
Rotor Blade thickness (midspan) [in]	0.0706	0.0544	0.0528	0.0505	0.0488	0.0456
Rotor Blades (R_{1-6})	16	20	20	25	28	32
Stator Blades (S_{1-6})	14	26	28	32	36	30

III. DATA ACQUISITION

A. DATA ACQUISITION SYSTEM (DAS)

1. Overview

The DAS in this research was comprised of five independent systems. Each system met a specific need to analyze a range of operating parameters and conditions. The *Superflow Data Acquisition (Model SF-901)* system was used to measure inlet air flow capacity, compressor speed (N_1), power turbine speed (N_2), engine torque and fundamental parameters required for normal engine operations. Similar to the *Superflow* DAS, the *HP 3852A Data Acquisition/Control Unit* recorded steady state parameters during engine operation. The next system acquired high frequency response data from the *Kulite* pressure transducers which were stored and analyzed using an *HP 3562A Dynamic Signal Analyzer (DSA)*. The same signals coming from the *Kulites* were observed using an *HP 54601* Oscilloscope as a raw voltage signal. The last data acquisition system was the *National Instruments* P.C. based A-to-D converter. Each of these systems will be described in detail.

2. Superflow Model SF-901 Data Acquisition

This system is a monitoring and control system manufactured by *Superflow Corporation (SF-901 Model)* (Figure 3.1). The *Superflow Model SF-901* is a water brake dynamometer power absorption unit controlled by a Superflow control console. This console monitors compressor and turbine speeds, output shaft speed and power, engine torque, and other pressures and temperatures, necessary to operate the engine. In addition to monitoring the engine, the console allows for mechanical control of both, the engine throttle power and power absorption by the water brake. The Data Acquisition System of the *SF-901* is initiated at the console and simultaneously stored in a P.C.. These data were used for analysis and calculation of the mass flow rates entering the compressor at

21

different testing speeds. (See Appendix B for further explanation of the calculated mass flow rates)

3. Hewlett-Packard 3852A Data Acquisition/Control Unit

The second system was used to measure 8 pressure and 57 thermocouple signals (Figure 3.1). These data were collected in the *Hewlett-Packard 3852A Data Acquisition/Control Unit* and transferred to a P.C. via a National Instruments IEEE 488-2 General Purpose Interface Bus (GPIB) for storage into a P.C.. Microsoft Excel was used for processing (See Appendix C). These data were used to measure average values for the compressor inlet total temperature (T_{T1}), compressor discharge total pressure (P_{T2}) and compressor discharge total temperature (T_{T2}). In turn, these values were used to calculate compressor efficiency and overall pressure ratios for the reference testing speeds.

4. HP 3562A Dynamic Signal Analyzer (DSA) Data Acquisition

This system used the Dynamic Signal Analyzer to measure the filtered signals from the flush mounted pressure transducers. Figure 3.2 shows a block diagram of the measurement chain.

The DSA is a waveform analyzer using an FFT based signal analyzer that allows measurement of signals in the time or frequency domain. The *HP 3562A* provides a 256 kHz sampling rate with a 20,480 sample buffer used during recording signals up to 100kHz. One feature used during testing, was the time-averaged data processing. In this experiment, 10 samples were averaged to obtain power spectra.

The softkey settings for the initial setup of the analyzer in the time domain were: "MEAS MODE" on "Time Capture" to observe data, then "AVG Start" to start averaging over 10 samples sizes.

22

The softkey settings for the initial setup in the frequency domain were: "MEAS DISP" on "PSD1" to observe the data, then "AVG Start" to start averaging over 10 samples sizes.

Once the average data were plotted, the data were transferred to a P.C. using a National Instruments IEEE 488-2 GPIB for storage and analysis with a MATLAB file. These data obtained from the DSA, were used to analyze and observe the blade-to-blade passing frequency at four different testing speeds 35,000 - 40,000 - 45,000 - 50,000 RPM and investigate any anomalies in the pressure distribution in the time or the frequency domain of each channel.

Time histories were recorded for the four channels at all speeds and power spectral density plots were used to investigate the blade passing frequency, rotor frequency, transducer natural response and any other unexpected frequencies.

5.   Hewlett-Packard 54601 Oscilloscope

The *HP* 54601 Oscilloscope provided a measurement of a raw signal from the signal amplifier and a single trace of the voltage vs. time plot. Figure 3.3 displays the equipment arranged during testing in the Marine Propulsion Laboratory.

6.   National Instruments AT-MIO-16F-5 A-to-D Card

This system allows for external signals to trigger data acquisition and clocking. This allows for phase-lock acquisition and ensemble averaging. The clocking signal is to be taken off the compressor blading to acquire data. A problem was encountered when using this system due to limited frequency response of the eddy current proximeter.

This card is a multi-functional input/output device with a sampling rate of 200 kHz, 12 bit, $\pm$ 5 volt yielding a 2.44 millivolt digital resolution that can have up to 8 differential channels or 16 open-ended channels. The data will be digitized and stored on a P.C..

23

Superflow Data Acquisition (Model SF-901)

HP 3862A Data Acquisition/Control Unit

Superflow Engine Control Console
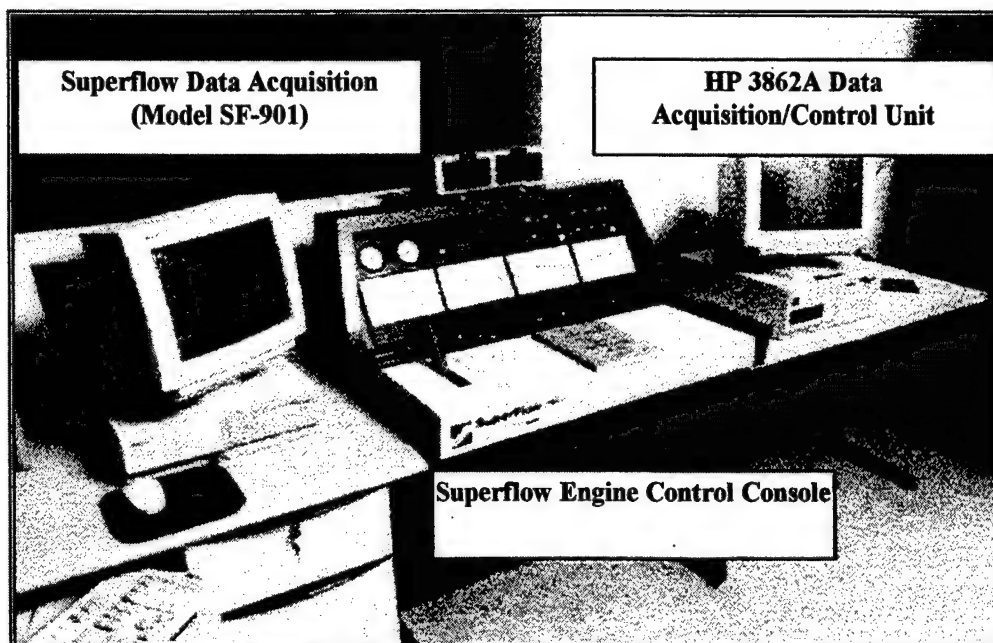
Figure 3.1 Data Acquisition and Operating Control System.
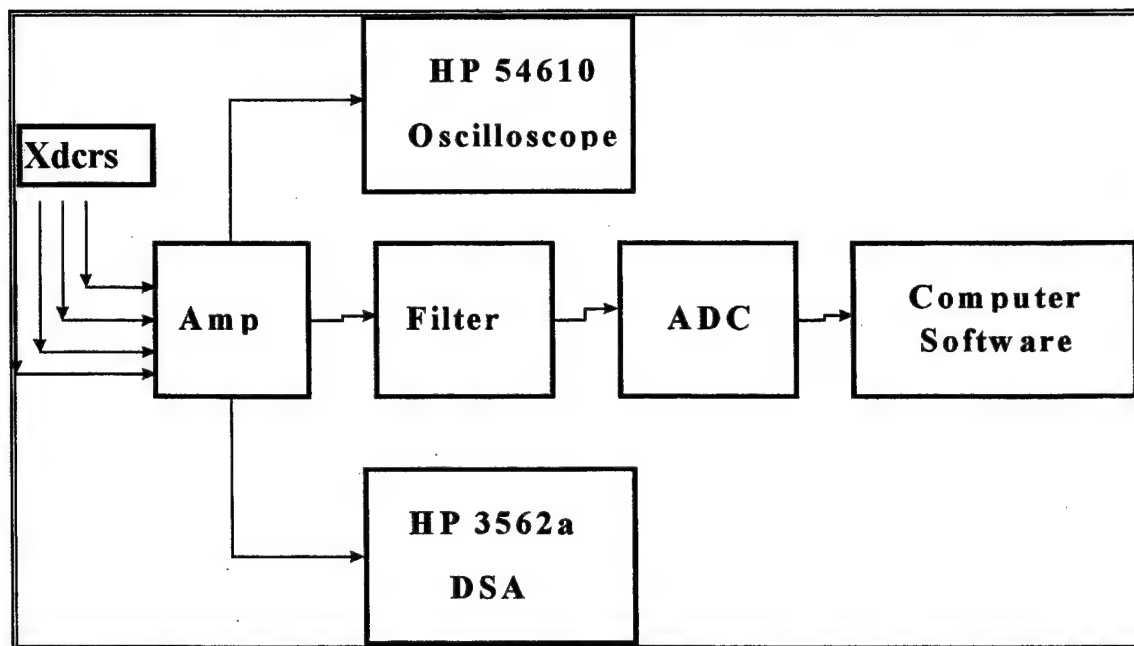
Figure 3.2 Block Diagram of the Measurement Chain for the Static Casing Pressures.
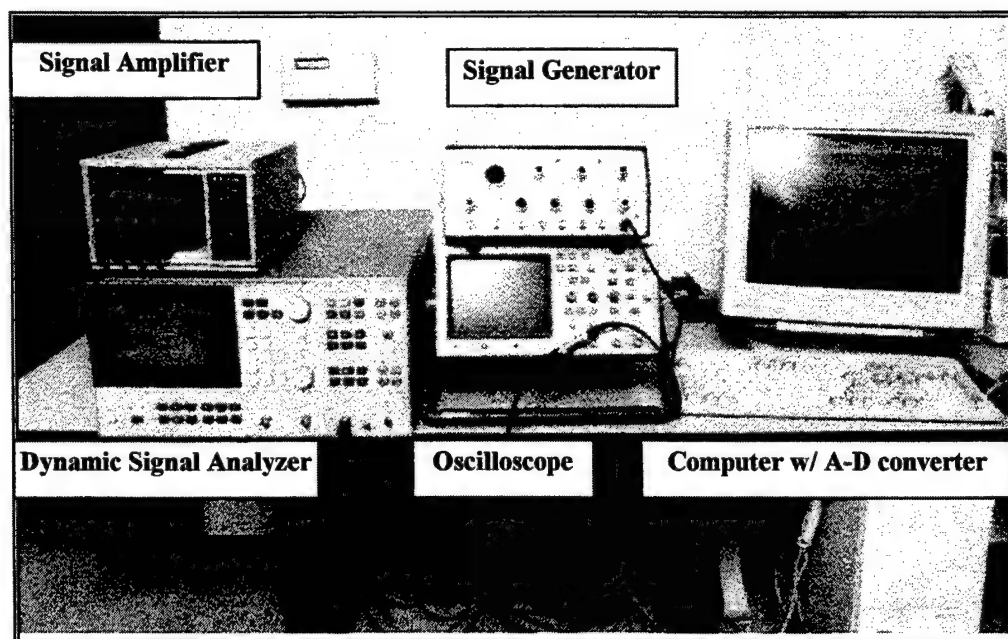
Figure 3.3 Data Acquisition for Casing Static Pressure Measurements.

25

IV. RESULTS

A.   OVERVIEW

Data were obtained for casing static pressures in the compressor for 35, 40, 45, 50 kRPM. Four data channels were used for each pressure transducer and time history and power spectrum plots were reported. The data obtained by the DSA as a pressure versus time history, were repeatable and consistent for all speeds. For simplicity, all the data to be presented below are for test runs at 50,000 RPM only, Appendix D provides the results for the other speeds.

Another set of data were obtained for the steady state performance characteristics of the compressor at various speeds. In particular, mass flow rates and inlet temperature and pressure conditions were reported.

B.   PRESSURE WAVE PATTERNS

A sawtooth wave form in the time domain was expected on both the oscilloscope and DSA before testing. Figure 4.1 shows a typical voltage versus time plot for one signal at the 2/3rd location of the compressor. This oscilloscope trace shows how the rising slope increases as the pressure side of the blades passes the stationary transducer. Note the similarity of a sawtooth waveform exhibited by the rising and falling slopes of the plot, indicating that the blade passing frequency was present.

The oscilloscope verified the passing of rotor blades were present at the anticipated frequency. This trace also captured the natural response of each pressure transducer which were nominally at 100 kHz.

27
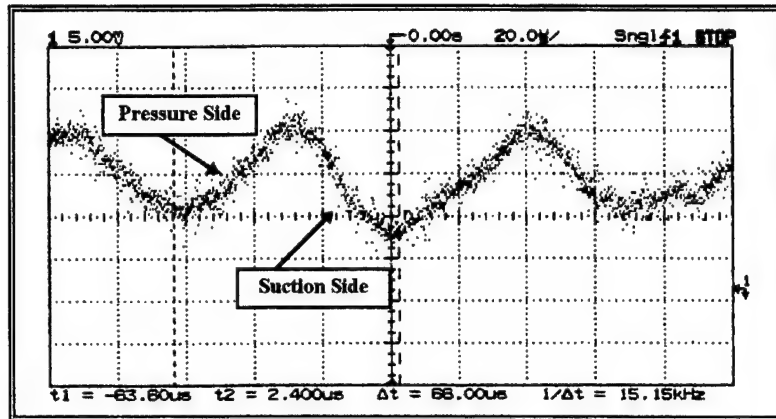
Figure 4.1 Oscilloscope Trace of Voltage vs. Time from Channel 4 at 45000 RPM and 2/3rd axial chord.

Inspection of the pressure versus time histories showed that pressure waveforms from the 1/3rd axial chord of the compressor (Channels 1 and 3) were nearly identical (Figure 4.2 and 4.3). The 2/3rd of the compressor rotor (Channels 2 and 4) had repeating waveforms, however a variation was evident (Figure 4.4 and 4.5).

The complete time history at Channels 2 and 4 shows an average amplitude (peak-to-peak) approximately equal to 3 and 3.75, respectively. Channels 1 and 3 remain constant at approximately 3 psi for both channels. This pressure difference between the suction side and pressure side of a blade was used to calculate the pressure coefficient, C_p = $(P_p-P_s) / (\frac{1}{2} \rho w^2)$, where $\frac{1}{2} \rho w^2$ = the dynamic head, w = the velocity relative to the blade at the leading edge and ρ = the density at the stage temperature. To compare the magnitude of C_p versus the axial chord, empirical data from Rains [Ref 5] were used. The nominal clearance can be extracted from Figure 4.6 (where λ in this Figure is the tip clearance / blade thickness). Using the following parameters:

w = 653 ft/sec and   thickness (t) = 0.0393 in   [Ref 33]

ρ = 0.08216 lbm/ft^3 (1.316 kg/m^3)

Channel 1 or 3 (P_p-P_s) = 3 psi

∴ C_p= 0.80 **which yields a nominal clearance about 4 mils**

Now conducting the same calculations for Channel 4 at (P_p-P_s) = 3.75 psi, located at the 2/3rd axial chord and using the previous values to determine C_p;

28

∴ **$C_p = 1.0$ which yields a nominal clearance about 3 mils**

Clearly, the variation of the peak-to-peak pressure amplitudes is directly related to the nominal clearance. based on [Ref 5] which used the typical wall pressure distribution for uniform tip clearances.

Therefore, whatever the imperfection that exists at the location near Channel 4 (not seen by Channel 2) causes a large pressure fluctuation near the trailing edge of the 2nd stage rotor blading. Any residual effects from other imperfections have no effect on this signal due to the energy density at this location.

C.   CASING PRESSURE POWER SPECTRA

The Power Spectral Densities (PSD) of the time varying voltage signals from all four casing pressure transducers were analyzed using the Dynamic Signal Analyzer (DSA). The signals were analyzed one channel at a time using averages of 10 time records. This averaging procedure was done to obtain maximum signal to noise ratio and have more repeatable measurements.

Figure 4.7 shows the PSD (un-normalized) versus frequency (in Hz) for both transducers 1 and 3, respectively. These transducers are for the 1/3rd axial chord location, 180 degrees apart. Just as with the time-domain signals, they are very similar. They show that the signal energy is concentrated at 3 distinct frequencies in this band. Namely, there is energy at low frequencies due to a D.C. offset and once per rotor revolution disturbances. The transducer on the bottom of the casing (Chan..3) shows more energy at rotor speed. There is a large spike at around 16.7 kHz and a smaller one at around 33.4 kHz for both. This energy is due to blade passing and the second harmonic of blade passing.

While not shown in these Figures, the natural frequency of the transducers can be seen on similar plots as energy at higher frequencies between 80 and 100 kHz. Each transducer has its own identifiable natural frequency.

Figure 4.8 shows the PSD (un-normalized) versus frequency (in Hz) for transducers 2 and 4 respectively. These transducers are for the 2/3rd axial chord location, 180 degrees apart. As expected, these PSDs are quite different. Most notably the magnitude of the energy at the blade passing frequency (16.7 kHz) is much larger for the transducer on the bottom part of the case (Chan.4) than on the top (Chan.3). Also many other frequencies are present including substantial energy at rotor speed.

The PSDs confirm the results of the time domain signals. Namely, that the pressures in the front part of the 2nd stage row are quite similar and independent of circumferential location while the pressures in the rear part of this row spatially as well as temporally varying.

D.   BASELINE COMPRESSOR PERFORMANCE

A reference set of steady state data were taken in this experiment for an "as is" compressor to characterize its performance at various speeds. The testing conditions and mathematical calculations for the values in Table 4.1-4.3 are described in Appendix B.

Table 4.1 reports the local pressures at the inlet and outlet of the compressor so as to characterize and state an operating pressure ratio and compressor efficiency for this turbomachine between the speeds of 35,000 - 50,000 RPM.

Table 4.2, reports the percent difference between the measured mass flow (using the turbine flow meters), the calculated mass flow rate at the bellmouth entrance, and compared these values to [Ref 32], the Allison Design Installation Manual. Note the disparity between the installed turbine flow meter and [Ref 32], which could indicate out of calibration flow meters or that the method of deriving the measured value through the Superflow data processing is not accurate. Additionally, it was noted that the turbine flow meters base their calculations on a Standard Temperature and Pressure are 60°F and 29.92"Hg, according to the Superflow Calibration Manual, instead of 68 °F.
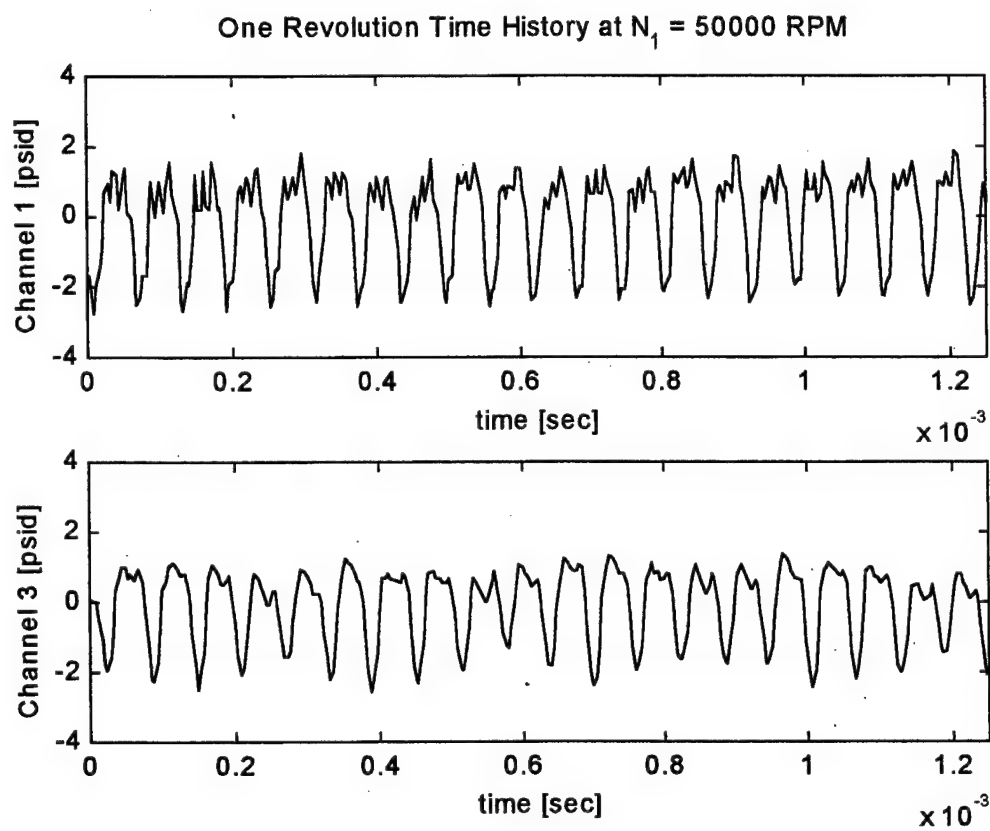
Figure 4.2 One Revolution Time History for Channels 1 and 3 at 50000 RPM.

31
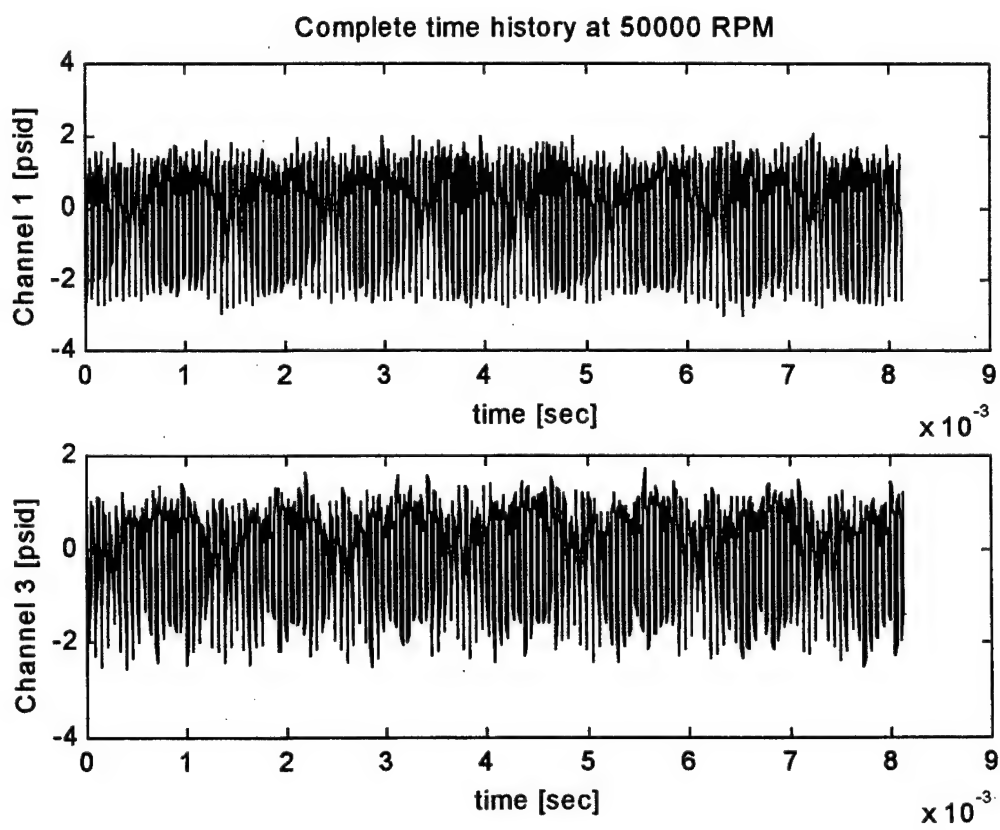
Figure 4.3 Complete Time History for Channels 1 and 3 at 50000 RPM.
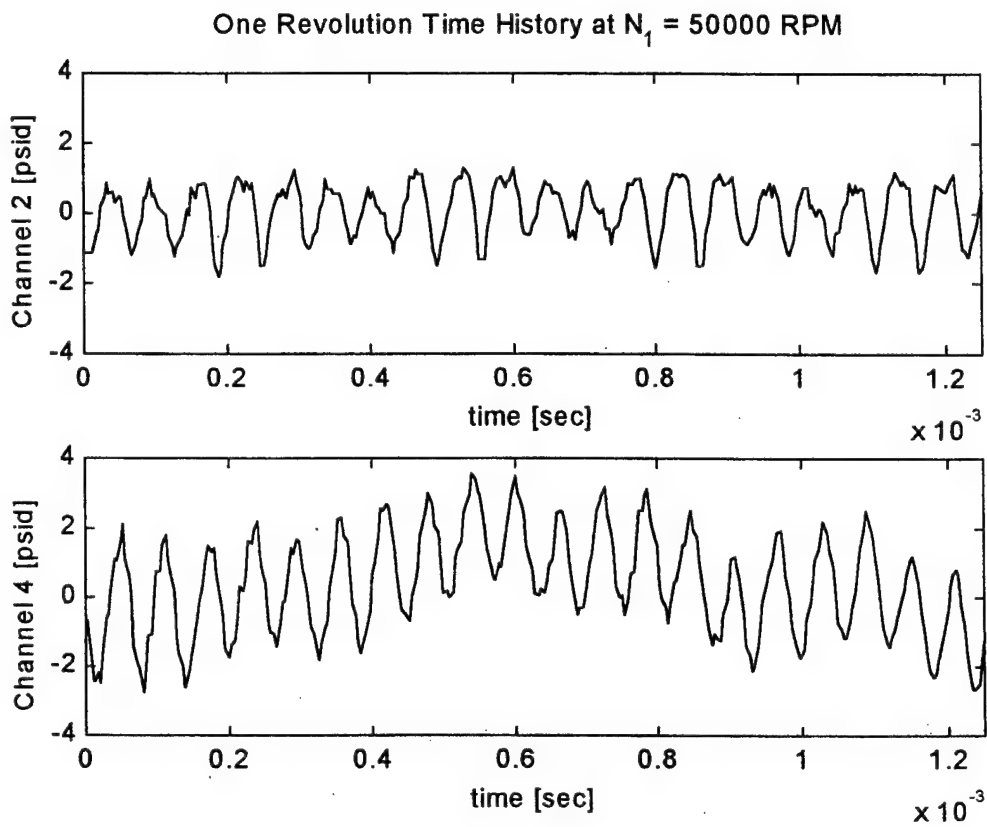
Figure 4.4 One Revolution Time History for Channels 2 and 4 at 50000 RPM.
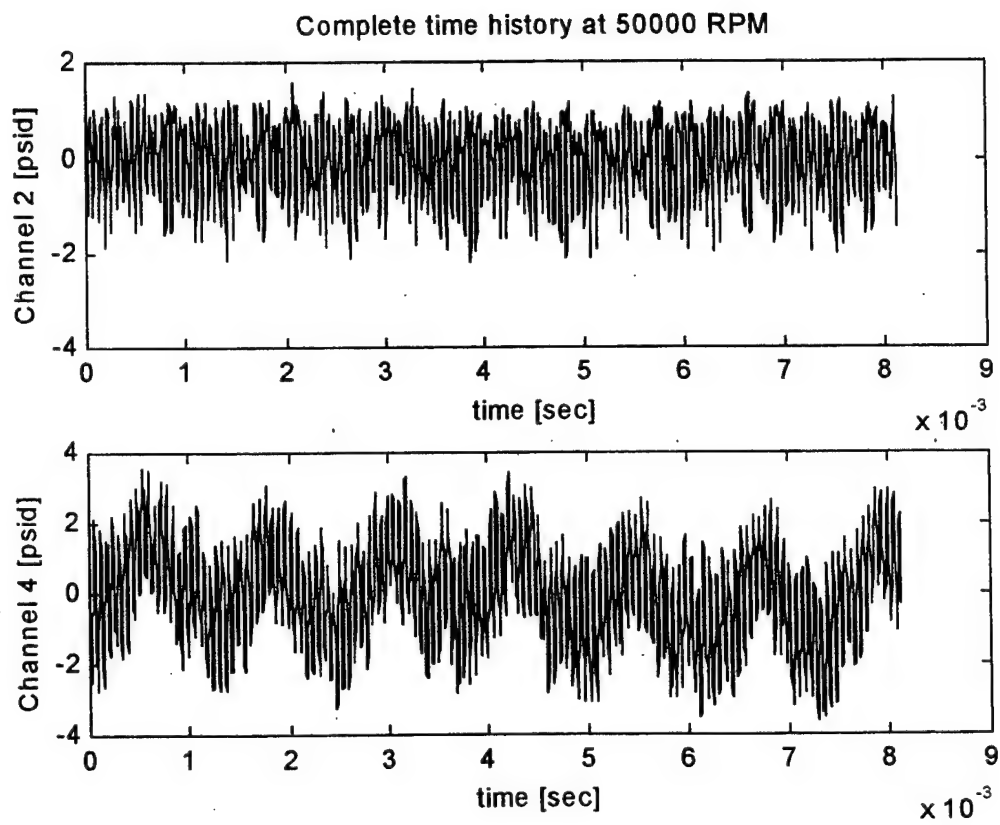
Figure 4.5 Complete Time History for Channels 2 and 4 at 50000 RPM.
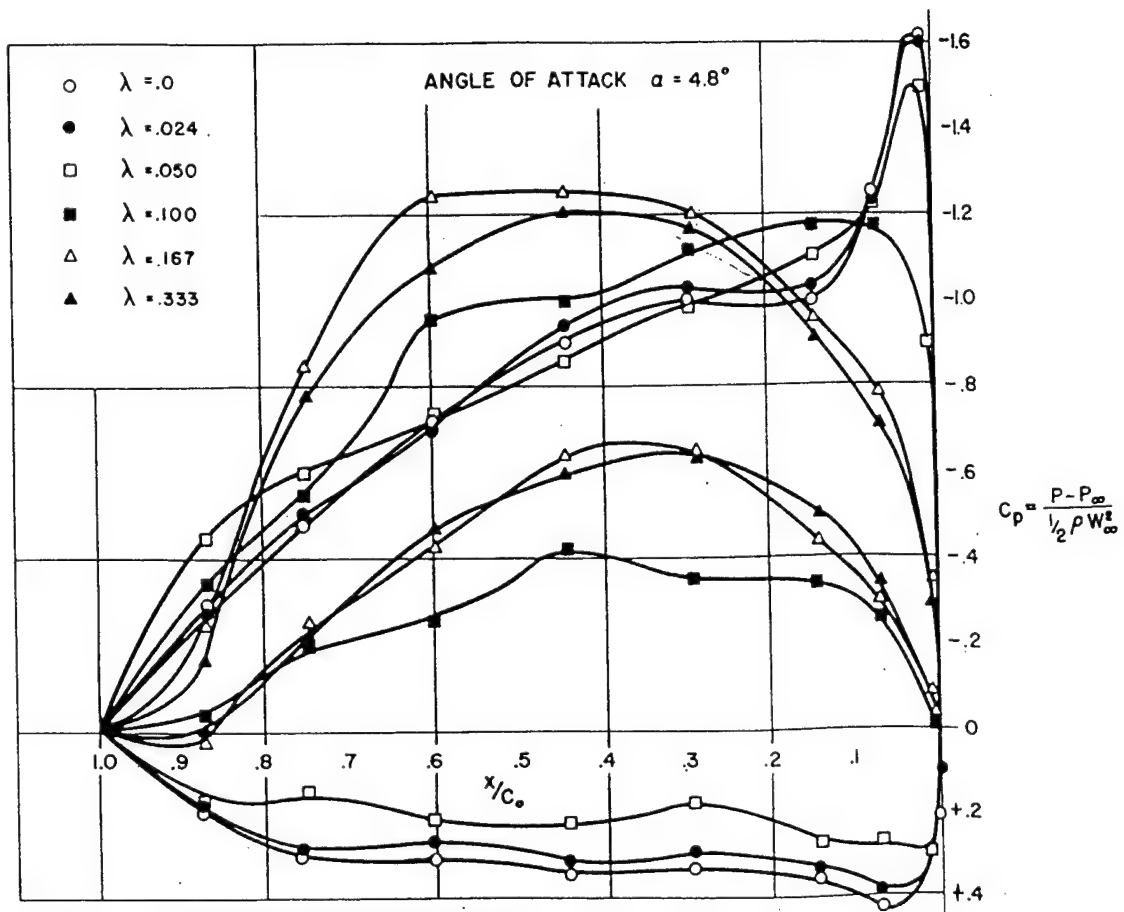
**Figure 4.6 Typical Wall Pressure Distribution Near the Tip of an Airfoil
Taken with permission from Rains [5].**
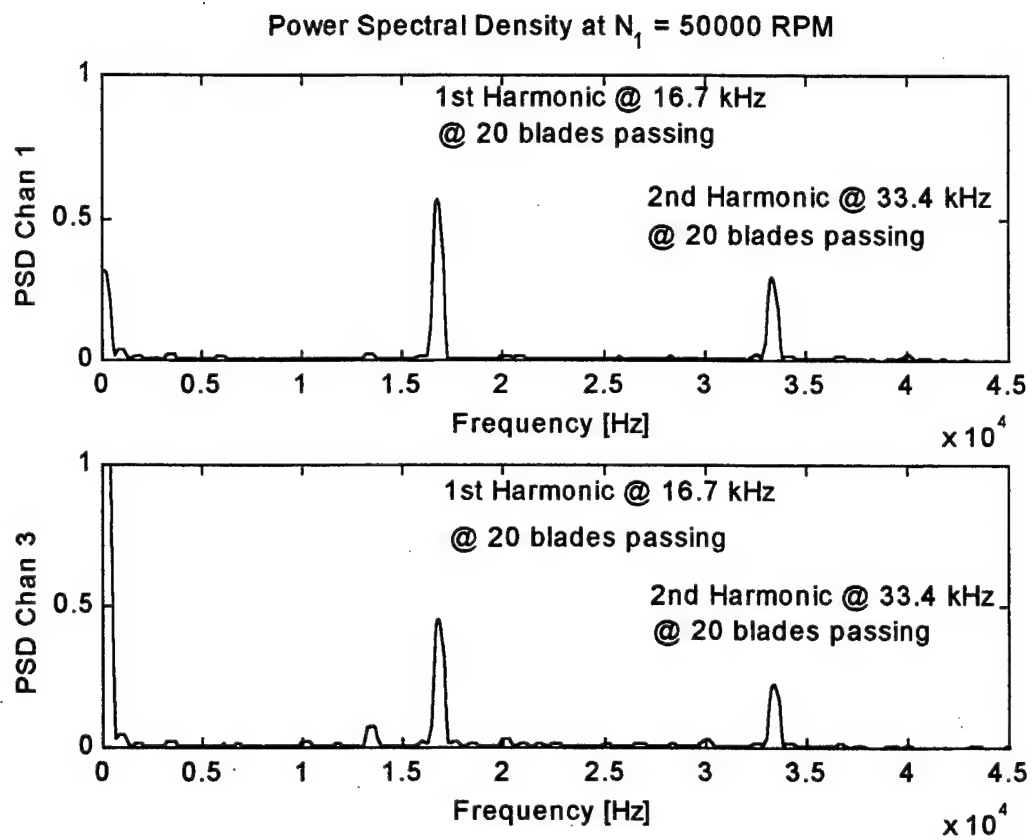
Figure 4.7 Power Spectral Density of Channels 1 and 3 at 50000 RPM.
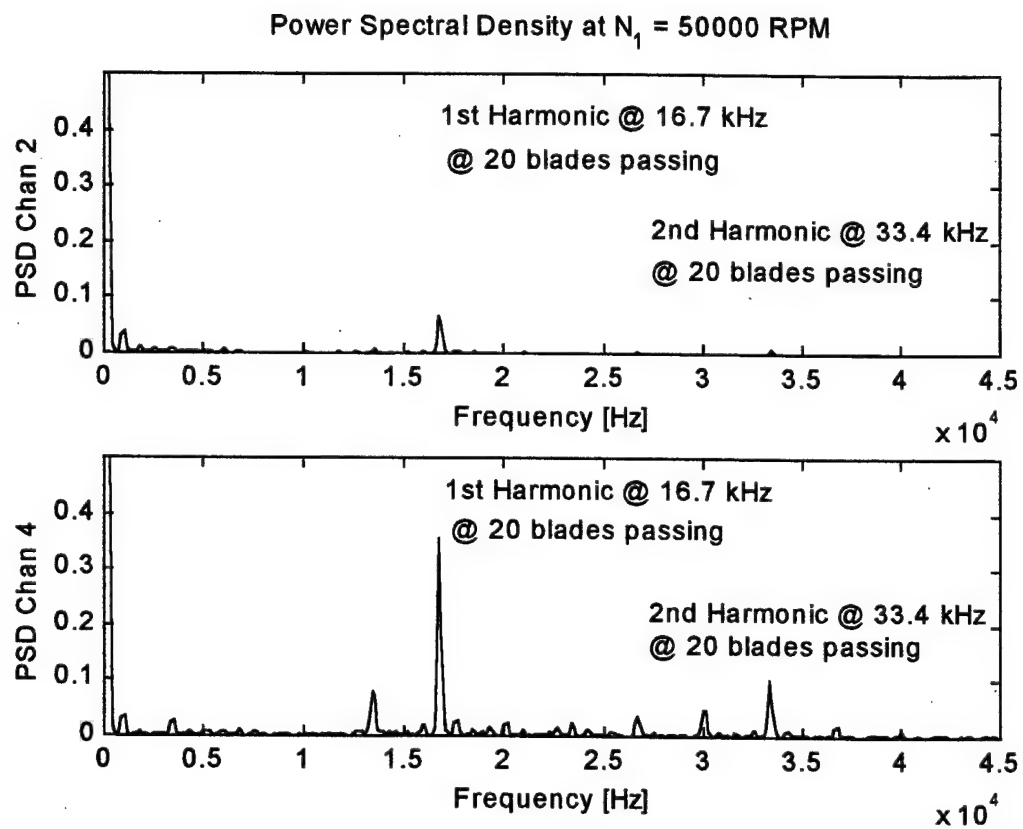
Figure 4.8 Power Spectral Density of Channels 2 and 4 at 50000 RPM.

Table 4.1 Allison T63-A-700 Baseline Engine Testing Data

Real Speed (RPM) N_1	Corrected Speed (RPM) N_{1corr}	Inlet Total Pressure (PSI) P_{T1}	Inlet Static Pressure (PSI) P_1	Comp. Disch Pressure (PSI) P_{T2}	π_c - P_{T2}/P_{T1}	Comp. Inlet Temperature (°F) T_{T1}	Comp. Disch Temperature (°F) T_{T2}	τ_c - T_{T1}/T_{T2}	η_c $\frac{\pi_c^{\wedge(\gamma-1/\gamma)}-1}{\tau_c-1}$
35000	34505	14.718	14.148	27.56	1.873	74.0	298.6	1.421	0.466
40000	39409	14.704	13.855	36.20	2.462	74.66	362.5	1.539	0.545
45000	44389	14.685	13.556	51.65	3.517	73.37	441.1	1.690	0.627
50000	49332	14.664	13.065	67.23	4.585	73.14	514.9	1.829	0.657

Table 4.2 Baseline Inlet Velocity and Mass Flow Condition Uncorrected Mass Flow Rate

(RPM) $N1_{corr}$	Turbine flowmeter* (LBM/SEC)	Compressible mass flow* (LBM/SEC)	Allison Design Manual* (LBM/SEC)	Axial Inlet Mach No.	C_z (FT/SEC)	Flow Coefficient ϕ
35239	1.884 (-1.9%)	1.920 (0%)	1.92	0.2382	266.78	0.454
40273	2.3062 (-0.59%)	2.317 (-0.13%)	2.32	0.2927	327.8	0.488
45307	2.6989 (2.2%)	2.638 (-0.08%)	2.64	0.3400	380.8	0.504
50341	3.2509 (5.5%)	3.078 (-0.06%)	3.08	0.4095	458.6	0.547

Table 4.3 Blade Passing Frequency and Rotor Frequency for the different test speeds

Compressor Speed N_1 [RPM]	Blade Passing Frequency (f_{blade}) [kHz]	Rotor Frequency (f_{rotor}) [Hz]
35000	11.7	583
40000	13.3	667
45000	15.0	750
50000	16.7	833

V. CONCLUSIONS AND RECOMMENDATIONS

A.   SUMMARY

A compressor casing was instrumented to measure time-resolved static pressures at 2 axial and 2 azimuth locations over the second stage rotor blades as they passed. Pressures at all 4 locations were recorded at several compressor speeds from 35,000 to 50,000 rpm. The 50,000 rpm runs were extensively analyzed.

The pressure versus time data were repeatable and consistent for all speeds. The 2 transducers located at the 1/3 axial chord showed nearly identical wave forms with most of the energy at blade passing frequency and lesser energy at the harmonics (mostly second harmonic) of blade passing. Some energy was present at rotor speed. The two pressures measured at the 2/3 axial chord on opposite sides of the casing showed very different wave forms. In particular, the one on the top of the compressor showed lower peak-to-peak amplitude and little energy at rotor speed while the pressure measured at the bottom of the case showed almost twice the blade passing amplitude and in addition, significant energy at rotor speed.

Additional instrumentation was installed and procedures were implemented for improved measurement of the steady state compressor performance. The mass flow measured with the calibrated bell mouth matched the values given in the Instillation Design Manual to within 1%. The mass flow measured by the turbine flow meters was different by several percent.

B.   CONCLUSIONS

The following conclusions have drawn from consideration of the data obtained:

1. The "as is" compressor has significant imperfections in the geometry of <u>both</u> the rotor and the stator. The rotor must be imperfect to create disturbances at rotor speed. In addition, the

41

casing must be imperfect and/or mis-aligned to have variations in measured pressure around the annulus at the same axial location.

2. The exact nature and magnitude of the combined imperfections is not known. It could be some combination of distortion and misalignment. However, it is probably true that the nominal rotor tip clearance on the front part of the second stage is about the same on the top as on the bottom. While the nominal tip clearance on the bottom part of the casing near the trailing edge is less than the top. This would explain why a fixed magnitude of rotor imperfection would produce both larger amplitude blade passing pulses and a much larger harmonic at rotor speed.

3. The phenomenon hypothesized at the outset of this program, namely that imperfect rotors can produce harmonics at rotor speed and hence generate synchronous forces, has been observed.

4. The instrumented bell mouth yields accurate measurements of engine air flow.

C.   RECOMMENDATIONS

Casing static pressure measurements should be taken both upstream and downstream of the second rotor row and compared the data already obtained. This should help to isolate the effect of the upstream flow disturbances.

It was found that significant imperfections (large enough to generate measurable pressure disturbances) exist in an "as is" compressor. In order to characterize the response due to an imposed imperfection only, all other imperfections must be eliminated or held constant. To make these type of measurements with confidence, techniques to measure the geometry insitu on an assembled compressor are necessary.

Problems arose in using an eddy current proximeter for data acquisition triggering and clocking due to inadequate frequency response. Other methods for triggering and clocking such as a capacitive probe should be investigated.

APPENDIX A

DIMENSIONS OF THE INSTRUMENTATION RING

The instrumentation ring is a split case configuration that is bolted through the compressor casing split line flanges. The ring is made of two halves, each specifically for one side of the compressor half.

One half of the Instrumentation Bridge

I.D	=	4.307 inches
Width	=	1.7 inches
Thickness	=	0.48 inches

Transducer Location

A total of nine ports were tapped. During operations, unused ports are sealed and plugged. To remove any part of the bridge, the engine must be secured and only the securing bolts should be removed. However, it is not recommended to remove the bridge unless both compressor casing halves are scheduled to be removed.

APPENDIX B

AIR FLOW CALCULATIONS

The gas turbine engine inlet is connected to an airbox plenum manufactured from ¼ inch transparent Plexiglass with a structural base for support. The airbox has the following characteristics:

Dimensions: (without the structural base)
          Length   72 inches
          Width   36.5 inches
          Height   36.5 inches

Flow Screens: (relative the air entering airbox 6 inches apart)
          1 inch diameter circular grating
          ½ inch diameter circular grating
          2 (two) honeycomb baffles
          20-mesh screen
          18-mesh screen

Superflow Airflow turbines:
2 (two) turbines wired in parallel
          Maximum: 2400 SCFM
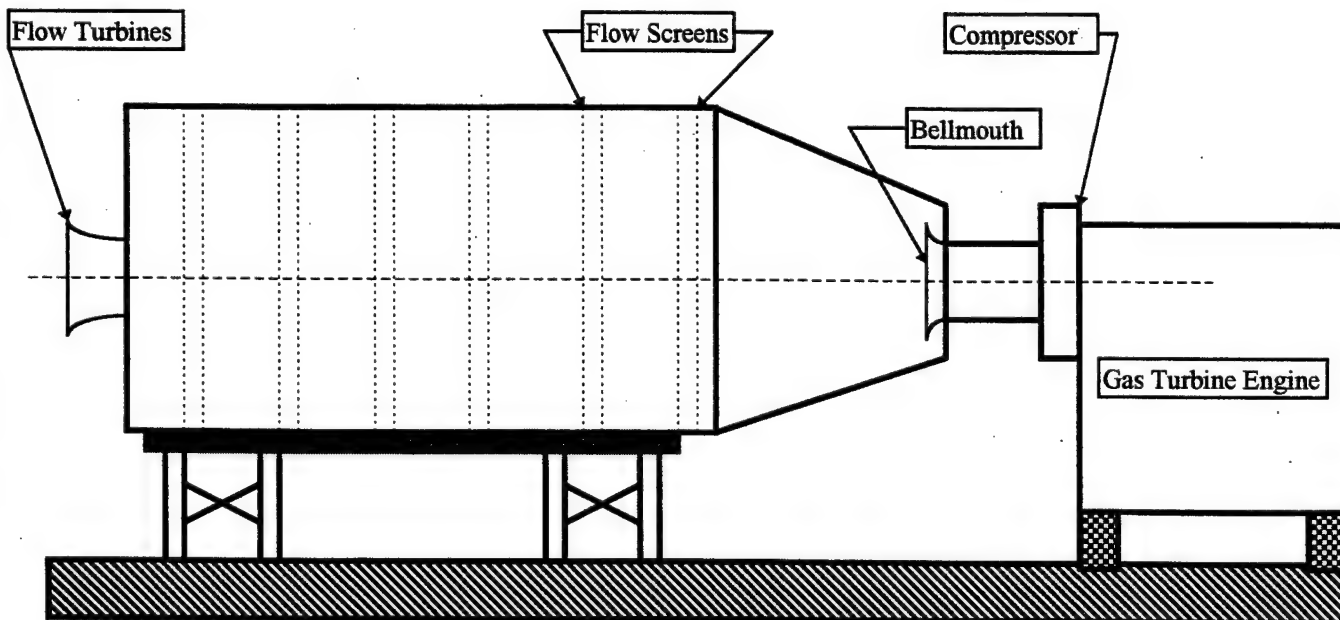
The values calculated in Table 4.1 used measured data from the compressor bellmouth, the *Superflow Data Acquisition System (SF-901)*, and the outlet conditions of the compressor airflow (P_{T2} and T_{T2}).

The *Superflow* airflow turbines on the inlet airbox measured the air flow capacity (Q_{air}). This volumetric flow rate [in SCFM] was converted to a mass flow rate in [LBM/SEC]. To verify the accuracy of the flow meters, a compressible flow equation derived from Bernoulli's equation was used. The MATLAB computer code (FILENAME: Massflow.m) included in this Appendix calculates all the values in Table 4.2.

From this point on, the mass flow rates had to be corrected and standardized to effectively compare the values to (STP) Standard Temperature and Pressure. To correct the mass flow rates, a temperature ratio (θ) and a pressure ratio (δ) were calculated as shown below. The corrected values of mass flow rates are reported in Table 4.1.

Corrected Parameters: Corrected parameters are used to normalize data obtained for different inlet conditions. The standard conditions are:

$$P_{std} = 101{,}325 \text{ Pa} \qquad (29.92 \text{ in Hg})$$
$$T_{std} = 288.15 \text{ K} \qquad (518.67°R)$$

Let $\quad \delta \equiv \dfrac{P_{in}}{P_{std}}$ and $\quad \theta \equiv \dfrac{T_{in}}{T_{std}}$ where P_{in} and T_{in} are the inlet states of the compressor

Corrected mass air flow $\quad = \quad \dfrac{\dot{m}_{airflow}\sqrt{\theta}}{\delta} \quad$; obtained from the Compressible Flow Equation

Corrected RPM ($N1_{corr}$) $\quad = \quad \dfrac{N}{\sqrt{\theta}}$

Compressible Air Flow equation: Derived from Bernoulli's Equation is defined as

$$\dot{m}_{airflow} = \frac{C_D p_{T1} A_{bell}}{\sqrt{RT_{T1}}} \cdot \pi_c^{\frac{1}{\gamma}} \cdot \sqrt{\frac{2\gamma}{\gamma-1}\left[1-\left(\pi_c\right)^{\gamma-\frac{1}{\gamma}}\right]}$$

where π_c = Total Compressor Pressure Ratio = $\dfrac{p_{T2}}{p_{T1}}$

    p_{T1} = Total compressor inlet pressure

    p_{T2} = Total compressor discharge pressure

    τ_c = Total Compressor Temperature Ratio = $\dfrac{\tau_{T2}}{\tau_{T1}}$

    T_{T1} = Total compressor inlet temperature

    T_{T2} = Total compressor discharge temperature

    C_D = Dischagre Coefficient of bellmouth

    A_{bell} = Minimum area of compressor bellmouth

    γ_{air} = Ratio of Specific Heats for air = 1.4

    R = Gas Constant for air @ 20° C = 287.15 J/K

    $\dot{m}_{COM-air}$ = compressible eqn mass flow rate

    $\dot{m}_{ACT-air}$ = Superflow mass flow rate

    Q_{air} = Volumetric flow rate of air

```matlab
clear
% Constants
A_bell = 0.009369;                          % Area of bellmouth (m^2)
C_d   = 0.98;                               % Discharge Coefficient of bellmouth
R_SI  = 287.15;                             % Gas Constant for Air (S.I.)
R_EN  = 53.34;                              % Gas Constant for Air (English)
T_std = 518.67;                             % Standard Temp in Rankine
P_std = 14.696;                             % Standard Pressure in psi
Gamma = 1.4;                                % Ratio of Specific Heats for Air


% Enter values as required
N_act  = input('Enter Actual Compressor Speed (rpm) = ');
AMB_PRESS = input('Enter Ambient Pressure (inches Hg) = ');
AMB_TEMP = input('Enter Ambient Temperature (degrees F) = ');
AMB_TEMP = AMB_TEMP + 460.67;               %degree Rankine
P_s   = input('Enter Static Pressure (psi) = ');
P_s   = P_s * 6894.7573;                    %Convert to Pascals
P_t   = input('Enter Total Pressure (psi) = ');
P_t   = P_t * 6894.7573;                    %Convert to Pascals
T     = input('Enter Total Temperature (degrees F) = ');
T     = ( (T-32)/1.8 )+ 273.15;             %Convert to Kelvin
Q_turb = input('Enter Volumetric Flow of Turbines (SCFM) = ');
m_turb = (Q_turb*((P_std)*2.4)/(R_EN*T_std))    % lbm/sec

% Calculate Incompressible mass flow in [lbm/sec]
Im_ideal = 2.2046 * (( P_s*A_bell ) / ( (R_SI*T)^.5 )) * (2*(P_t - P_s)/P_s )^.5
Im_real  = C_d * m_ideal


% Calculate the Inlet Mach Number, Inlet Velocity, Flow Coefficient
M_in = (((P_t/P_s)^((Gamma-1)/Gamma) - 1 )* (2/(Gamma-1)) )^0.5
c = sqrt(Gamma*T*R_SI);
Vel_in  = M_in * c
Phi = Vel_in/(N_actual/60)


% Calculate Compressible mass flow in [lbm/sec]
Cm_ideal = 2.2046 * A_bell*P_t*sqrt(Gamma)*M_in/sqrt(R_SI*T) * ...
(1/(1+ ((Gamma-1)/2) *M_in^2))^3
Cm_real = C_d * Cm_ideal

% Pressure correction factor - DELTA
STD_PRESS = 29.61 * 2.03602;                % S.T.P in psia
Delta = AMB_PRESS / STD_PRESS;

% Temperature correction factor - THETA
Theta = AMB_TEMP/T_std;                     %Correction factor
m_dot_CORR1 = (m_turb * sqrt(Theta)) / (2.03602 * Delta)
m_dot_CORR2 = (m_real * sqrt(Theta)) / (2.03602 * Delta)

% Calculate Corrected Speed
N_CORR = N_act / sqrt(Theta)
```

APPENDIX C

DATA ACQUISITION FILES

Chan No.	Description of measurement			Compressor Speed N1 = 35000 rpm				
				1st Run	2nd Run	3rd Run	4th Run	AVG Values
1	Compressor inlet temperature (degrees F)			71.91	74.21	76.56	76.99	74.92
2	Compressor inlet temperature (degrees F)			69.72	72.28	74.68	75.62	73.07
3	Compressor discharge temp (degrees F)			294.50	301.41	301.82	303.55	300.32
4	Compressor discharge temp (degrees F)			291.65	297.75	298.49	299.70	296.90
5	Gas generator inlet temp (degrees F)			1315.19	1322.33	1324.98	1312.25	1318.69
6	(Thermocouples 5-20 read the inner radii)			1327.02	1338.39	1337.42	1332.98	1333.95
7				1390.54	1375.01	1368.35	1366.82	1375.18
8				1470.36	1482.80	1473.85	1487.21	1478.55
9				1346.83	1354.26	1356.12	1366.80	1356.00
10				1272.79	1267.46	1263.79	1274.21	1269.56
11				1238.66	1206.57	1206.91	1211.28	1215.86
12				1079.32	969.10	968.89	1001.39	1004.67
13				1124.59	1118.82	1115.28	1122.07	1120.19
14				1138.94	1132.71	1126.83	1132.45	1132.73
15				1183.97	1166.06	1163.85	1168.28	1170.54
16				1225.73	1201.36	1198.58	1197.06	1205.68
17				1172.24	1159.28	1158.09	1164.53	1163.53
18				1170.83	1156.76	1164.21	1164.43	1164.06
19				1178.90	1177.87	1183.31	1180.10	1231.59
20				1220.87	1232.95	1239.24	1233.30	1231.59
21	Gas generator inlet temp (degrees F)			1354.78	1376.16	1379.79	1372.89	1370.91
22	(Thermocouples 21-37 read at mid radii)			1421.26	1437.93	1433.01	1433.97	1431.54
23				1444.88	1464.69	1470.68	1469.22	1462.37
24				1505.82	1528.36	1517.51	1533.00	1521.17
25				1391.67	1399.79	1400.34	1420.41	1403.05
26				1315.95	1311.78	1309.18	1325.66	1315.64
27				1221.85	1210.30	1217.31	1222.22	1217.92
28				1126.77	1121.88	1120.00	1125.06	1123.43
29				1113.26	1101.39	1102.57	1106.70	1105.98
30				1166.16	1148.23	1139.51	1146.39	1150.07
31				1223.54	1203.55	1186.31	1195.52	1202.23
32				1239.38	1212.19	1220.35	1216.85	1222.19
33				1183.30	1159.57	1165.71	1172.61	1170.30
34				1142.84	1135.14	1134.90	1170.36	1145.81
35				1175.38	1184.18	1187.55	1238.46	1196.39
36				1283.99	1284.36	1297.58	1407.38	1318.33
37				1412.93	1406.17	1415.81	1555.11	1447.51
38	Gas generator inlet temp (degrees F)			1453.16	1449.29	1453.00	1621.53	1494.24
39	(Thermocouples 38-52 read the outer radii)			1472.19	1451.96	1496.86	1659.82	1520.21
40				1485.76	1524.40	1509.50	1698.91	1554.64
41				1367.18	1392.02	1373.68	1608.31	1435.30
42				1243.56	1213.51	1222.45	1384.71	1266.06
43				1178.13	1171.75	1164.92	1357.50	1218.07
44				1107.59	1102.19	1099.73	1242.21	1137.93
45				1124.23	1104.84	1102.68	1240.55	1143.07
46				1148.63	1115.26	1105.18	1224.57	1148.41
47				1222.77	1208.06	1195.02	1330.21	1239.02
48				1270.37	1270.74	1273.26	1412.86	1306.81

49					1168.53	1148.56	1144.69	1264.38	1181.54
50					1145.40	1140.56	1136.28	1251.66	1168.48
51					1190.48	1203.17	1191.60	1320.70	1226.49
52					1310.69	1311.45	1293.19	1443.10	1339.61
53	Power turbine inlet temperature (degrees F)				944.03	945.10	950.67	1009.74	962.39
54	Power turbine exit temperature (degrees F)				795.40	786.80	785.87	819.90	796.99
55	(Thermocouples 55-57)				0.00	0.00	0.00	0.00	0.00
56					0.00	0.00	0.00	0.00	0.00
57					0.00	0.00	0.00	0.00	0.00
58	Channels 58-61 reserved for future testing				79.62	98.50	102.02	101.63	95.44
59					79.57	98.05	101.51	101.25	95.09
60					79.77	97.09	100.54	100.37	94.44
61					7.87	7.98	7.88	10.95	8.67
62	Compressor discharge pressure (psia)				25.20	25.30	25.14	34.47	27.53
63	Compressor discharge pressure (psia)				25.20	25.41	25.17	34.53	27.58
64	Gas generator inlet pressure (psia)				47.97	48.59	48.09	48.42	48.27
65	Gas generator inlet pressure (psia) FAULTY				0.00	0.00	0.00	0.00	0.00
66	Power turbine inlet pressure (psia)				4.25	4.32	4.28	6.43	4.82
67	Power turbine inlet pressure (psia)				3.88	3.92	3.87	6.08	4.44
68	Power turbine exhaust pressure (psia)				0.14	0.17	0.18	0.19	0.17
69	Power turbine exhaust pressure (psia)				0.22	0.25	0.25	0.26	0.25

Chan No.	Description of measurement				Compressor Speed N1 = 40000 RPM				
									AVG Values
1	Compressor inlet temperature (degrees F)				72.88	76.34	77.34	75.78	75.58
2	Compressor inlet temperature (degrees F)				70.50	74.21	74.67	75.53	73.73
3	Compressor discharge temp (degrees F)				360.68	366.11	365.74	516.66	402.29
4	Compressor discharge temp (degrees F)				356.70	362.03	361.54	514.04	398.58
5	Gas generator inlet temp (degrees F)				1483.94	1474.67	1469.73	1884.78	1578.28
6	(Thermocouples 5-20 read the inner radii)				1485.21	1490.39	1474.90	1862.09	1578.15
7					1524.32	1526.32	1503.64	1870.80	1606.27
8					1615.36	1610.13	1608.48	1947.89	1695.46
9					1465.20	1474.32	1470.10	1808.13	1554.44
10					1379.09	1383.15	1381.14	1740.11	1470.87
11					1329.27	1321.04	1314.75	1701.33	1416.60
12					1085.53	1068.92	1077.53	1440.04	1168.00
13					1239.26	1235.13	1245.70	1654.28	1343.59
14					1256.42	1252.77	1258.74	1667.75	1358.92
15					1287.79	1285.84	1290.91	1711.93	1394.12
16					1324.27	1318.67	1322.42	1793.94	1439.82
17					1293.70	1280.95	1289.27	1743.43	1401.84
18					1294.04	1295.63	1297.33	1754.72	1410.43
19					1317.72	1333.18	1325.48	1775.45	1437.96
20					1388.34	1396.15	1397.73	1820.66	1500.72
21	Gas generator inlet temp (degrees F)				1551.47	1538.53	1556.52	1972.68	1654.80
22	(Thermocouples 21-37 read at mid radii)				1594.88	1584.29	1601.71	1999.16	1695.01
23					1616.55	1611.41	1611.26	1999.47	1709.67
24					1640.36	1645.66	1627.19	1964.29	1578.99
25					1487.24	1496.01	1475.14	1857.56	1578.99
26					1399.58	1401.35	1406.18	1803.45	1502.64
27					1305.63	1308.18	1320.96	1731.79	1416.64
28					1231.53	1233.99	1239.18	1667.73	1343.11
29					1238.86	1229.97	1233.60	1686.71	1347.28
30					1276.94	1278.47	1279.29	1726.06	1390.19
31					1322.13	1318.13	1332.57	1776.21	1437.26
32					1341.96	1335.29	1342.34	1817.07	1459.17
33					1293.33	1290.97	1290.59	1768.91	1410.95
34					1267.69	1268.13	1269.08	1730.18	1383.77
35					1344.24	1342.58	1331.45	1777.44	1448.93
36					1464.33	1464.00	1453.87	1899.28	1570.37
37					1583.27	1575.13	1573.41	1992.88	1681.17
38	Gas generator inlet temp (degrees F)				1627.43	1611.49	1613.70	2000.34	1713.24
39	(Thermocouples 38-52 read the outer radii)				1628.32	1612.61	1637.55	1999.34	1719.45
40					1613.85	1590.96	1593.25	1929.25	1681.83
41					1469.93	1473.73	1480.90	1845.82	1567.59
42					1343.18	1341.48	1355.18	1806.65	1461.62
43					1266.52	1269.65	1272.14	1691.64	1374.99
44					1217.15	1208.78	1226.31	1667.65	1329.97
45					1241.90	1226.97	1246.37	1683.61	1349.71
46					1254.32	1231.77	1237.46	1625.25	1337.20
47					1318.93	1340.58	1322.18	1815.24	1449.23
48					1364.61	1367.80	1381.27	1774.31	1472.00

49						1270.86	1277.23	1274.05	1749.29	1392.86
50						1271.92	1287.51	1285.35	1732.69	1394.37
51						1369.26	1370.91	1390.49	1812.06	1485.68
52						1491.26	1477.01	1495.14	1920.53	1595.99
53	Power turbine inlet temperature (degrees F)					1006.80	1003.90	1009.18	1305.83	1081.42
54	Power turbine exit temperature (degrees F)					896.13	894.46	895.34	1118.83	951.19
55	(Thermocouples 54-57)					795.03	798.46	800.34	1031.69	856.38
56						815.09	815.49	820.37	1014.14	866.27
57						894.18	895.30	896.43	1001.39	921.83
58	Channels 58-61 reserved for future testing					87.04	99.89	100.58	108.30	98.95
59						87.31	99.74	100.21	108.20	98.86
60						87.46	99.51	99.62	108.55	98.79
61						11.38	11.40	11.36	20.51	13.67
62	Compressor discharge pressure (psia)					36.19	36.20	36.02	66.16	43.64
63	Compressor discharge pressure (psia)					36.21	36.19	35.98	66.45	43.71
64	Gas generator inlet pressure (psia)					47.13	46.27	47.49	11.25	38.04
65	Gas generator inlet pressure (psia) FAULTY					-0.09	-0.07	-0.07	-0.07	0.00
66	Power turbine inlet pressure (psia)					6.79	6.81	6.76	14.87	8.81
67	Power turbine inlet pressure (psia)					6.43	6.48	6.42	14.58	8.47
68	Power turbine exhaust pressure (psia)					0.19	0.19	0.20	0.22	0.20
69	Power turbine exhaust pressure (psia)					0.28	0.24	0.28	0.32	0.28

Chan No.	Description of measurement					Compressor Speed N1 = 45000 rpm				
						1st Run	2nd Run	3rd Run	4th Run	AVG Values
1	Compressor inlet temperature (degrees F)					71.66	71.45	71.93	74.87	72.48
2	Compressor inlet temperature (degrees F)					71.36	73.78	75.38	76.47	74.25
3	Compressor discharge temp (degrees F)					439.61	441.36	443.00	444.16	442.03
4	Compressor discharge temp (degrees F)					436.91	440.16	441.41	441.94	440.10
5	Gas generator inlet temp (degrees F)					1624.84	1619.92	1631.33	1622.86	1624.74
6	(Thermocouples 5-20 read the inner radii)					1637.31	1621.08	1628.89	1630.01	1629.32
7						1683.58	1657.82	1665.99	1668.72	1669.03
8						1720.55	1739.22	1740.33	1721.40	1730.37
9						1563.46	1581.29	1583.15	1566.01	1573.48
10						1494.10	1502.54	1517.28	1494.62	1502.13
11						1458.10	1451.31	1445.50	1443.16	1449.52
12						1155.34	1203.01	1217.24	1242.56	1204.54
13						1417.94	1420.59	1418.08	1424.62	1420.30
14						1448.15	1443.11	1448.88	1454.67	1448.70
15						1484.18	1470.66	1491.62	1476.56	1480.75
16						1525.58	1515.31	1515.39	1515.58	1517.96
17						1477.94	1464.25	1473.85	1463.46	1469.87
18						1479.44	1465.30	1479.11	1469.72	1480.34
19						1499.40	1491.34	1505.04	1497.50	1498.32
20						1552.92	1544.23	1563.66	1553.96	1553.69
21	Gas generator inlet temp (degrees F)					1701.58	1695.77	1702.98	1705.28	1713.81
22	(Thermocouples 21-37 read at mid radii)					1756.22	1746.05	1736.16	1754.90	1748.33
23						1776.61	1764.30	1761.00	1775.64	1769.39
24						1740.17	1746.01	1746.06	1746.35	1744.65
25						1599.97	1593.36	1615.72	1615.16	1606.05
26						1527.74	1526.70	1538.60	1568.18	1540.31
27						1442.26	1454.12	1458.20	1498.33	1463.23
28						1398.43	1404.82	1408.64	1466.28	1419.54
29						1424.47	1430.63	1421.64	1495.10	1442.96
30						1476.51	1475.95	1458.88	1542.53	1488.47
31						1523.49	1526.00	1510.23	1592.67	1538.10
32						1517.31	1530.15	1523.86	1636.73	1552.01
33						1470.93	1473.99	1472.12	1595.19	1503.06
34						1450.27	1450.94	1455.04	1558.50	1478.68
35						1516.06	1513.86	1521.83	1614.37	1541.53
36						1620.79	1615.98	1620.87	1720.63	1644.57
37						1739.45	1718.94	1729.54	1825.61	1753.38
38	Gas generator inlet temp (degrees F)					1779.12	1772.12	1779.61	1860.00	1794.00
39	(Thermocouples 38-52 read the outer radii)					1766.43	1756.12	1797.25	1879.98	1799.94
40						1672.92	1685.63	1711.09	1808.09	1719.43
41						1567.92	1579.78	1589.07	1728.86	1616.41
42						1548.45	1546.48	1550.19	1680.34	1581.36
43						1418.51	1429.18	1430.07	1598.69	1469.11
44						1406.05	1415.09	1412.45	1575.65	1452.31
45						1440.43	1450.15	1448.19	1613.72	1488.12
46						1428.70	1434.07	1424.60	1568.52	1463.97
47						1520.60	1514.14	1521.56	1725.50	1570.45
48						1476.01	1494.06	1503.94	1707.93	1545.48

49					1456.79	1457.85	1462.20	1667.92	1511.19
50					1460.17	1469.16	1466.93	1642.73	1509.75
51					1549.73	1549.94	1549.76	1689.76	1584.80
52					1651.39	1639.64	1650.69	1785.43	1681.79
53	Power turbine inlet temperature (degrees F)				1099.88	1104.96	1104.67	1224.45	1133.49
54	Power turbine exit temperature (degrees F)				1016.22	1013.69	1019.26	1043.98	818.63
55	(Thermocouples 54-57)				871.64	871.99	874.58	925.68	885.97
56					862.41	865.92	865.76	917.23	877.83
57					870.83	873.01	874.07	910.38	882.07
58	Channels 58-61 reserved for future testing				95.11	101.28	102.67	104.41	100.87
59					95.08	101.18	102.57	104.27	100.78
60					95.49	101.08	102.37	104.10	100.76
61					16.04	16.13	16.11	19.18	13.49
62	Compressor discharge pressure (psia)				51.65	51.68	51.72	61.40	54.11
63	Compressor discharge pressure (psia)				51.54	51.73	51.62	61.38	54.07
64	Gas generator inlet pressure (psia)				58.07	49.33	51.04	57.06	53.87
65	Gas generator inlet pressure (psia) FAULTY				-0.08	-0.08	-0.08	-0.07	0.00
66	Power turbine inlet pressure (psia)				10.82	10.85	10.81	13.62	11.52
67	Power turbine inlet pressure (psia)				10.44	10.51	10.47	13.26	11.17
68	Power turbine exhaust pressure (psia)				0.23	0.23	0.24	0.24	0.24
69	Power turbine exhaust pressure (psia)				0.28	0.24	0.24	0.25	0.26

Chan No.	Description of measurement					Compressor Speed N1 = 50000 rpm				
						1st Run	2nd Run	3rd Run	4th Run	AVG Values
1	Compressor inlet temperature (degrees F)					71.44	72.53	75.78	74.53	73.25
2	Compressor inlet temperature (degrees F)					73.67	69.87	75.53	70.85	73.03
3	Compressor discharge temp (degrees F)					515.25	514.74	516.66	515.78	515.55
4	Compressor discharge temp (degrees F)					514.89	513.77	514.04	514.64	514.24
5	Gas generator inlet temp (degrees F)					1875.85	1894.46	1884.78	1890.50	1885.03
6	(Thermocouples 5-20 read the inner radii)					1863.62	1868.21	1862.09	1864.22	1864.64
7						1884.12	1867.03	1870.80	1867.03	1873.98
8						1959.14	1952.79	1947.89	1956.89	1953.27
9						1804.56	1795.52	1808.13	1809.23	1802.73
10						1752.27	1749.69	1740.11	1751.33	1747.36
11						1722.38	1717.63	1701.33	1710.34	1713.78
12						1311.66	1396.18	1440.04	1398.21	1382.63
13						1661.59	1666.13	1654.28	1663.35	1660.67
14						1682.49	1684.28	1667.75	1689.09	1671.20
15						1715.34	1718.37	1711.93	1715.23	1715.21
16						1774.54	1782.78	1793.94	1788.12	1783.75
17						1754.42	1750.52	1743.43	1753.23	1749.46
18						1755.33	1768.84	1754.72	1770.23	1759.63
19						1772.74	1789.48	1775.45	1788.13	1779.22
20						1821.09	1843.08	1820.66	1848.30	1828.28
21	Gas generator inlet temp (degrees F) ·					1958.34	1975.48	1972.68	1973.29	1968.83
22	(Thermocouples 21-37 read at mid radii)					1990.29	1999.80	1999.16	1999.32	1996.41
23						1987.34	1984.52	1999.47	1984.48	1990.44
24						1951.84	1955.50	1964.29	1955.63	1957.21
25						1843.21	1857.36	1857.56	1857.92	1852.71
26						1802.57	1814.25	1803.45	1802.12	1806.76
27						1745.35	1743.13	1731.79	1744.28	1740.09
28						1679.12	1665.19	1667.73	169.25	1670.68
29						1696.18	1671.30	1686.71	1676.32	1684.73
30						1725.65	1695.98	1726.06	1699.10	1715.90
31						1772.55	1751.24	1776.21	1750.16	1766.67
32						1816.97	1817.67	1817.07	1820.23	1817.23
33						1780.31	1777.36	1768.91	1777.36	1775.53
34						1738.53	1744.60	1730.18	1756.23	1737.77
35						1784.15	1790.63	1777.44	1799.13	1784.08
36						1890.62	1898.98	1899.28	1899.45	1896.29
37						1985.76	1995.13	1992.88	1998.12	1991.25
38	Gas generator inlet temp (degrees F)					2019.08	2009.61	2000.34	2008.24	2009.68
39	(Thermocouples 38-52 read the outer radii)					1877.79	1959.76	1999.34	1960.93	1945.63
40						1918.90	1939.57	1929.25	1945.23	1929.24
41						1842.11	1853.47	1845.82	1855.42	1847.13
42						1793.32	1806.74	1806.65	1800.23	1802.24
43						1700.25	1687.53	1691.64	1692.83	1693.14
44						1668.27	1665.39	1667.65	1668.99	1667.10
45						1683.32	1696.30	1683.61	1696.30	1687.75
46						1638.66	1649.30	1625.25	1649.20	1637.74
47						1823.08	1813.02	1815.24	1819.36	1817.11
48						1765.03	1775.56	1774.31	1770.94	1771.63

49						1750.02	1744.33	1749.29	1755.32	1747.88
50						1733.58	1734.28	1732.69	1740.29	1733.52
51						1809.19	1816.33	1812.06	1812.34	1812.53
52						1858.37	1922.77	1920.53	1923.09	1900.56
53	Power turbine inlet temperature (degrees F)					1313.99	1298.86	1305.83	1299.43	1306.23
54	Power turbine exit temperature (degrees F)					1111.02	1113.19	1118.83	1114.30	1114.34
55	(Thermocouples 54-57)					1028.98	1033.30	1031.69	1038.39	1031.32
56						1008.56	1011.09	1014.14	1013.39	1011.26
57						996.67	999.20	1001.39	1001.13	999.09
58	Channels 58-61 reserved for future testing					101.71	106.05	108.30	103.23	105.35
59						101.35	105.93	108.20	105.23	105.16
60						101.09	105.96	108.55	108.23	105.20
61						20.86	20.86	20.51	20.86	20.74
62	Compressor discharge pressure (psia)					67.96	67.58	66.16	67.57	67.23
63	Compressor discharge pressure (psia)					67.94	67.34	66.45	67.84	67.24
64	Gas generator inlet pressure (psia)					51.39	15.01	11.25	15.01	25.89
65	Gas generator inlet pressure (psia) FAULTY					0.00	0.00	0.00	0.00	0.00
66	Power turbine inlet pressure (psia)					15.36	15.27	14.87	15.27	15.17
67	Power turbine inlet pressure (psia)					15.12	15.00	14.58	15.19	14.90
68	Power turbine exhaust pressure (psia)					0.26	0.26	0.22	0.25	0.25
69	Power turbine exhaust pressure (psia)					0.29	0.28	0.32	0.29	0.30

APPENDIX D

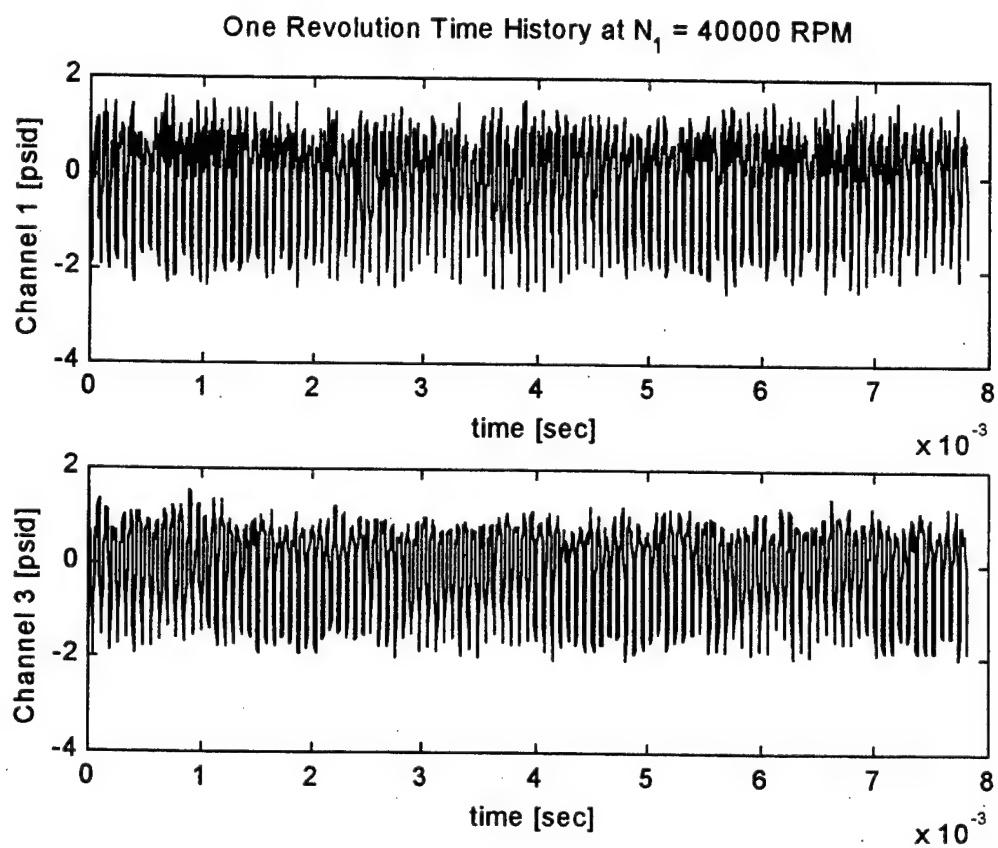## TIME HISTORY AND POWER SPECTRUM DATA PLOTS
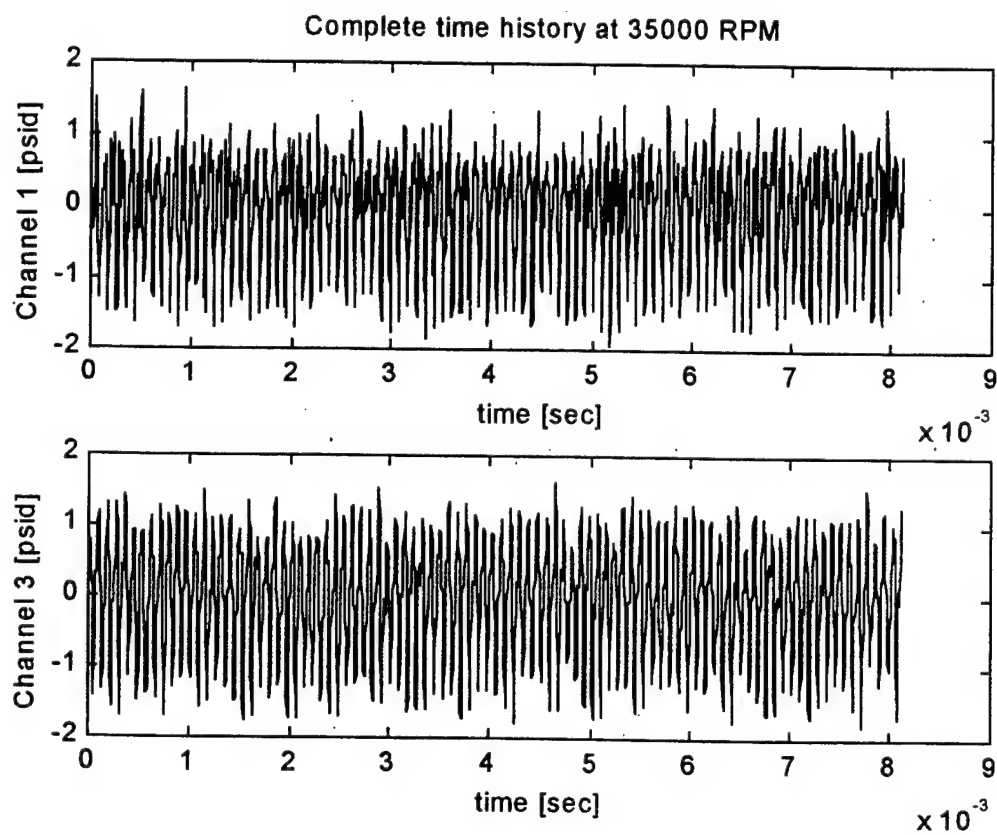
Complete Time History for Channels 1 and 3 at 35000 RPM.
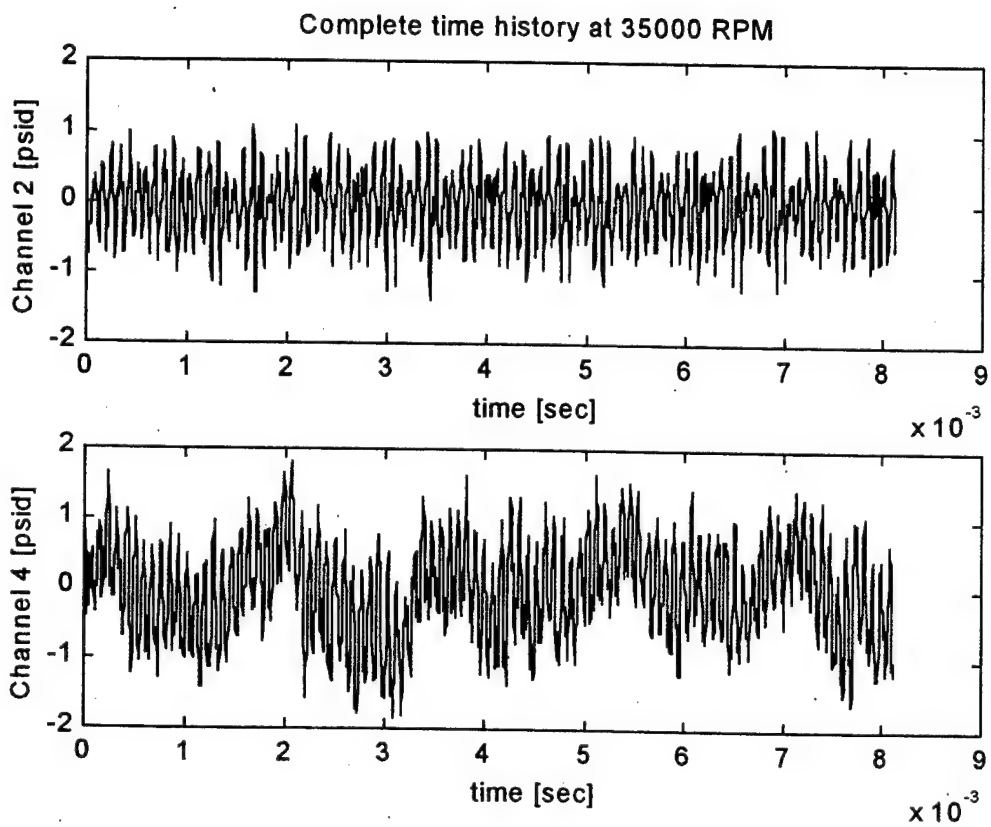
Complete time history at 35000 RPM

Complete Time History for Channels 2 and 4 at 35000 RPM

61

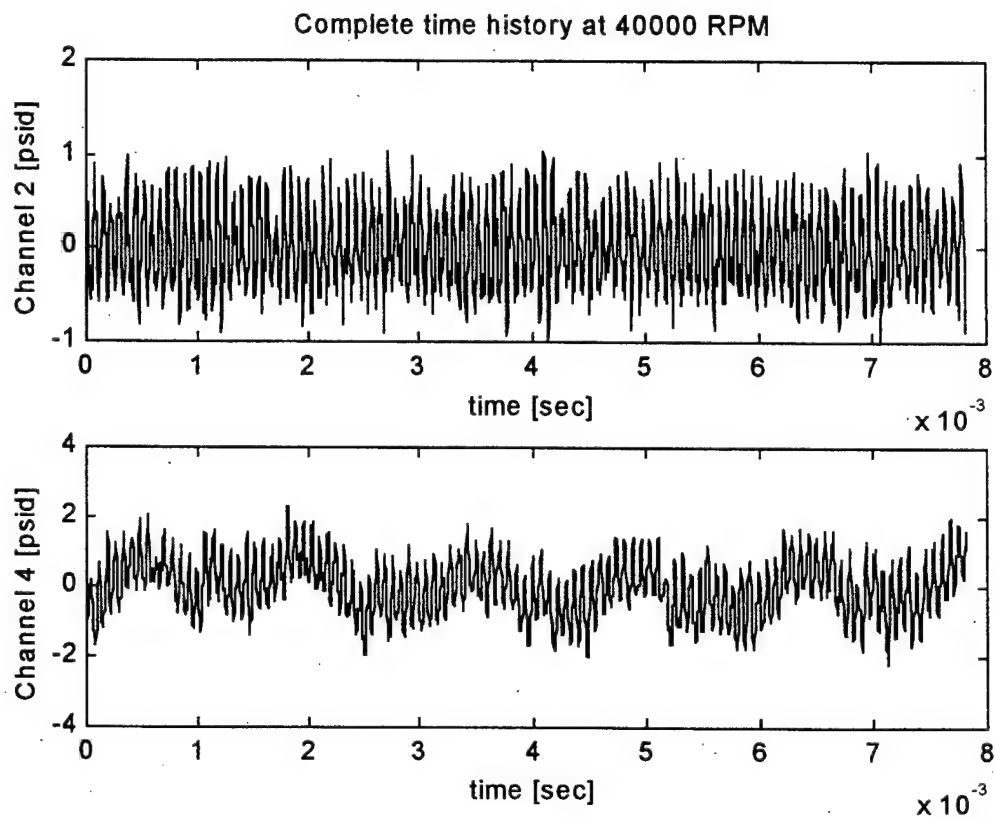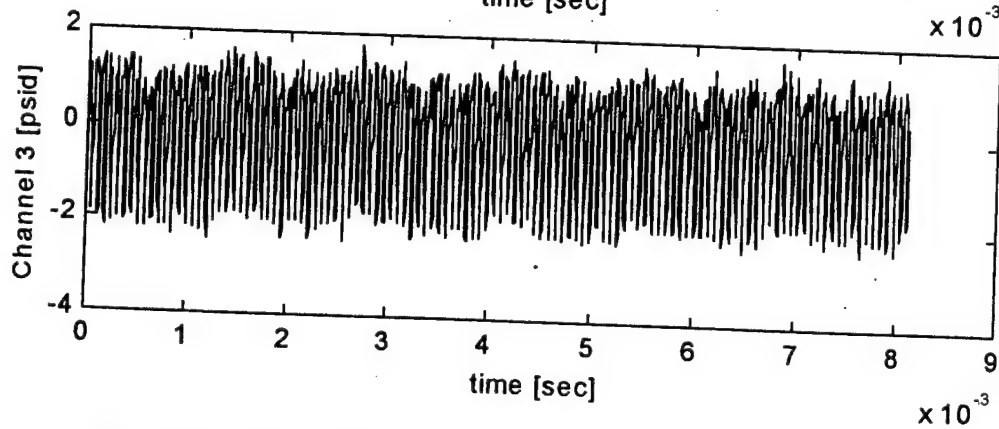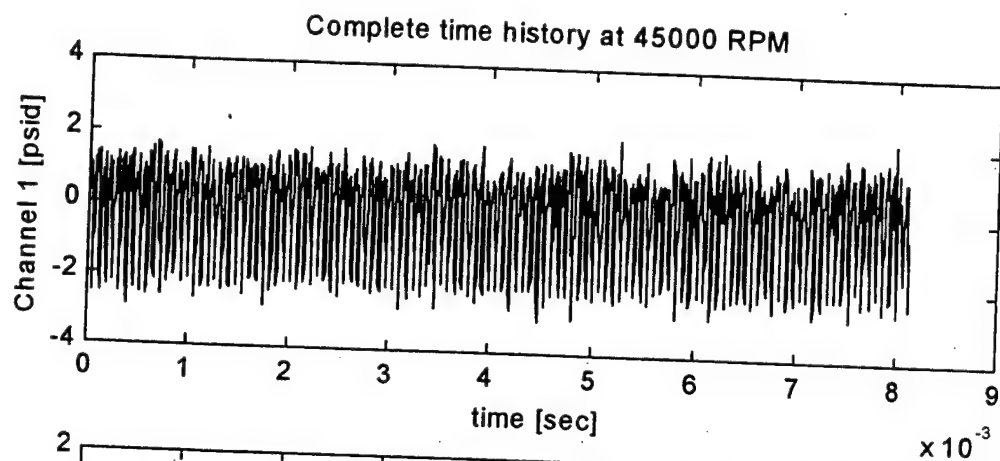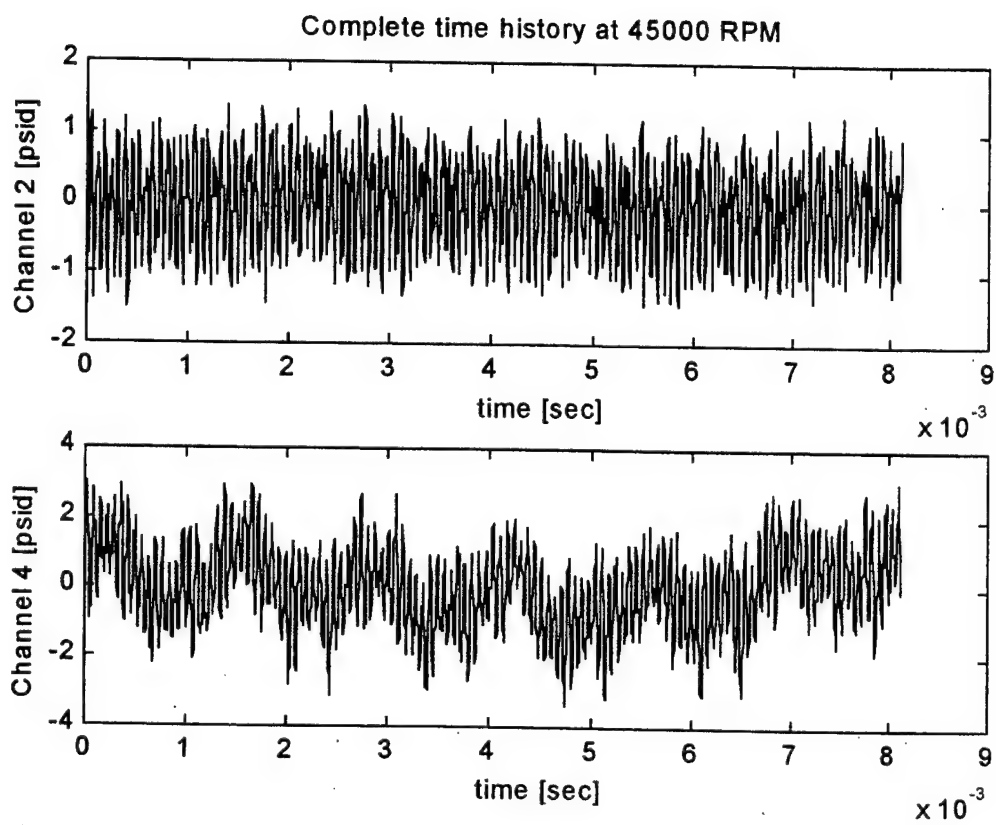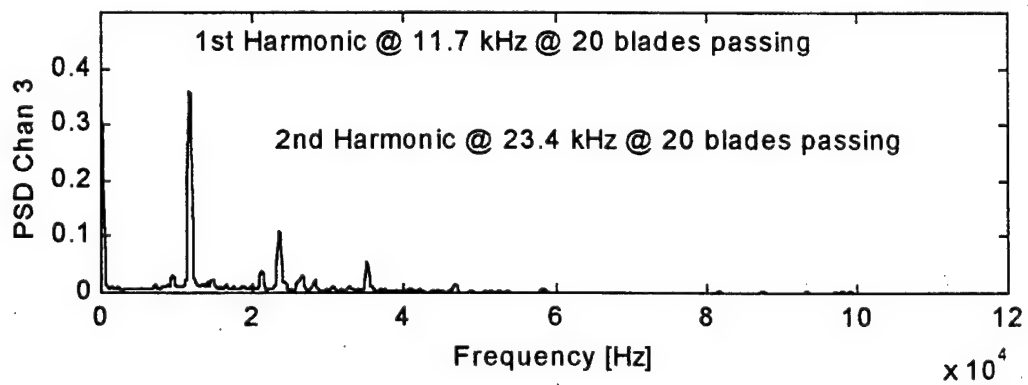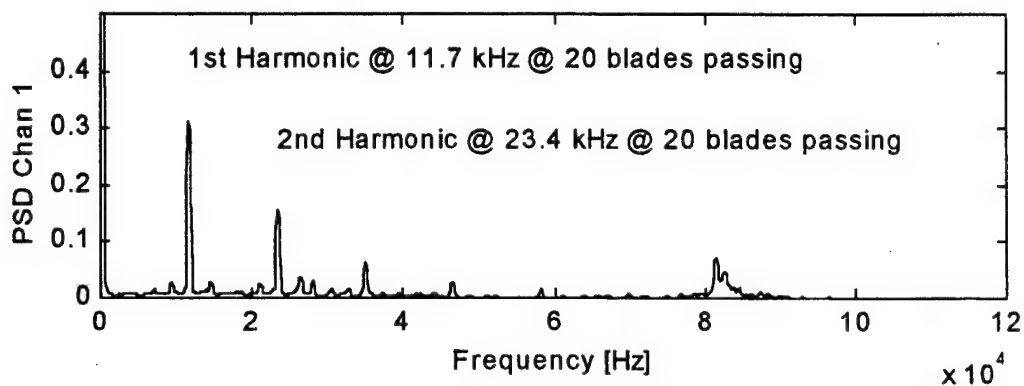One Revolution Time History at N_1 = 40000 RPM

Complete Time History for Channels 1 and 3 at 40000 RPM.

Complete Time History for Channels 2 and 4 at 40000 RPM
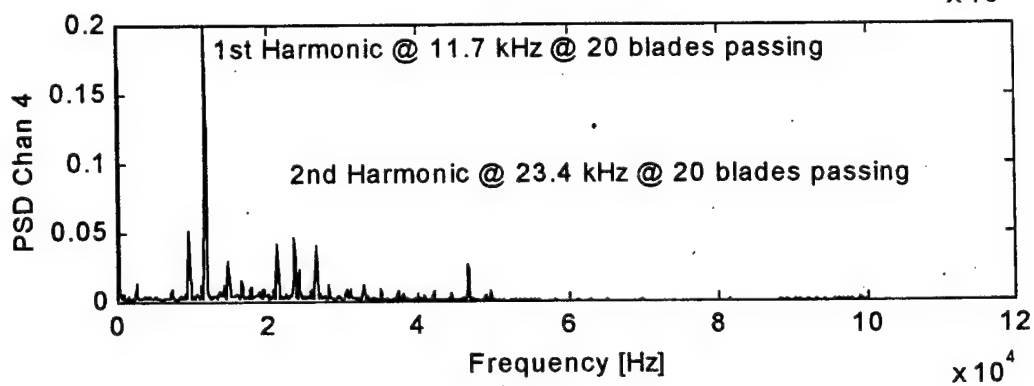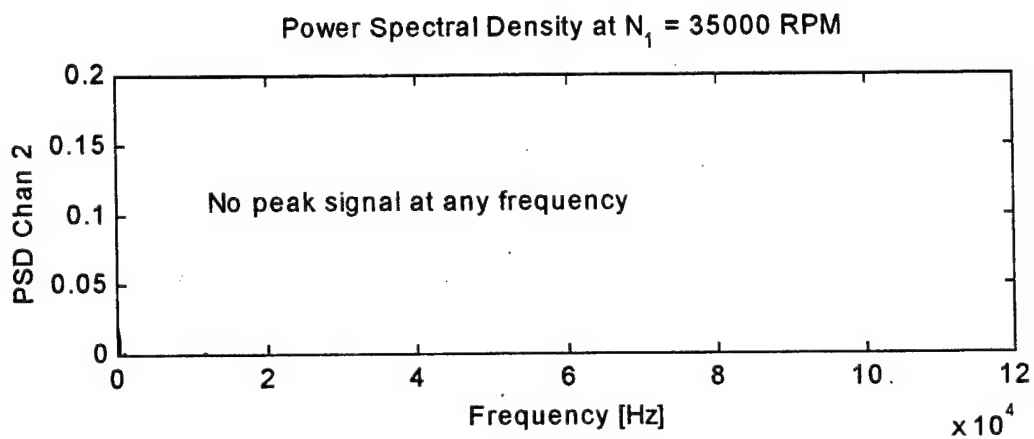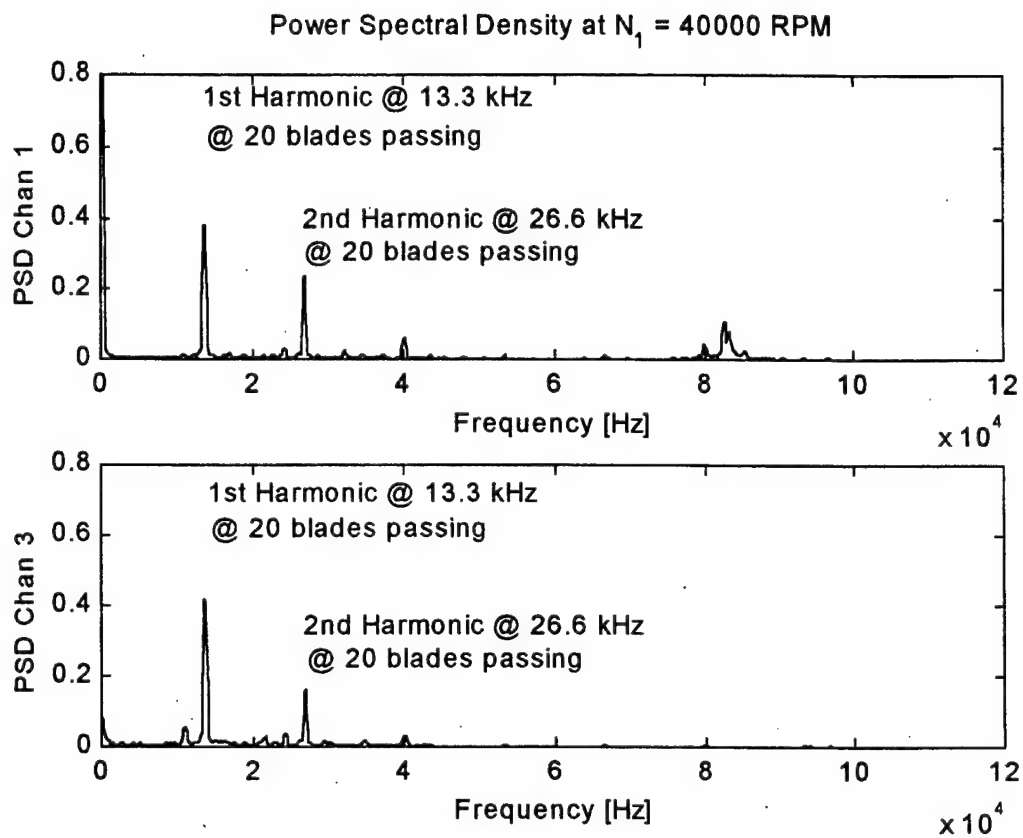
Complete Time History for Channels 1 and 3 at 45000 RPM

Complete time history at 45000 RPM

Complete Time History for Channels 2 and 4 at 45000 RPM

Power Spectral Density of Channels 1 and 3 at 35000 RPM

Power Spectral Density at N_1 = 35000 RPM

No peak signal at any frequency

1st Harmonic @ 11.7 kHz @ 20 blades passing

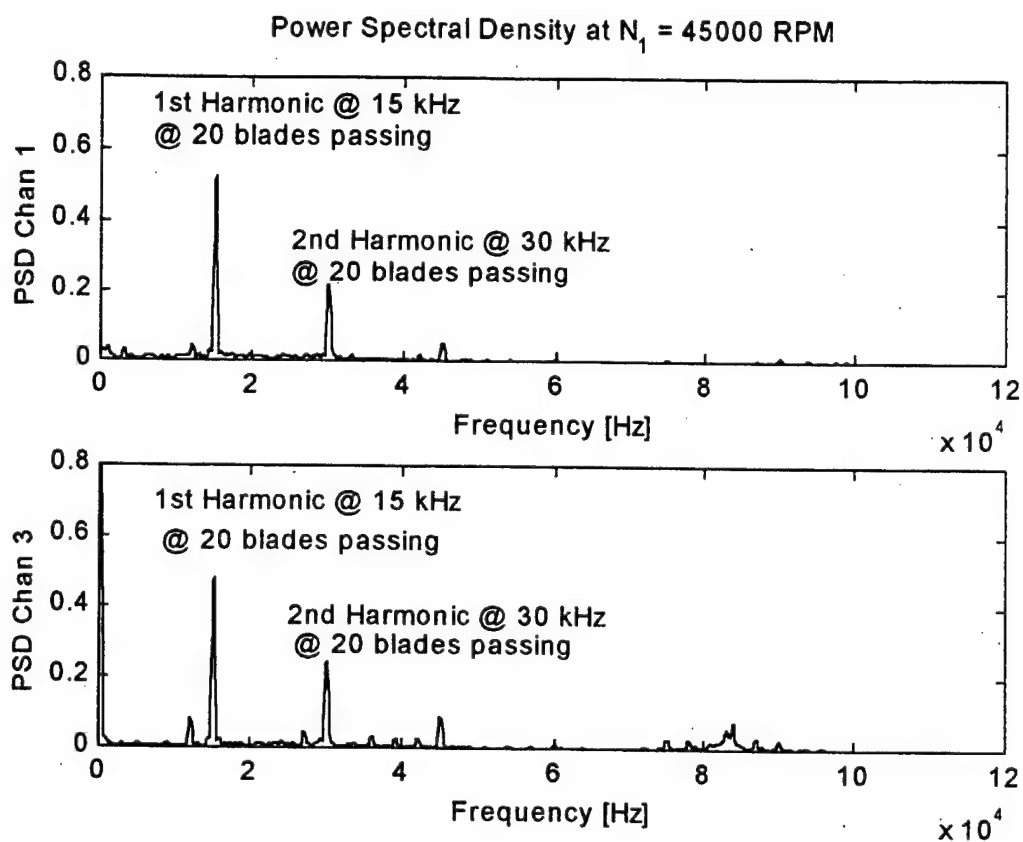2nd Harmonic @ 23.4 kHz @ 20 blades passing

Power Spectral Density of Channels 2 and 4 at 35000 RPM

Power Spectral Density of Channels 1 and 3 at 40000 RPM
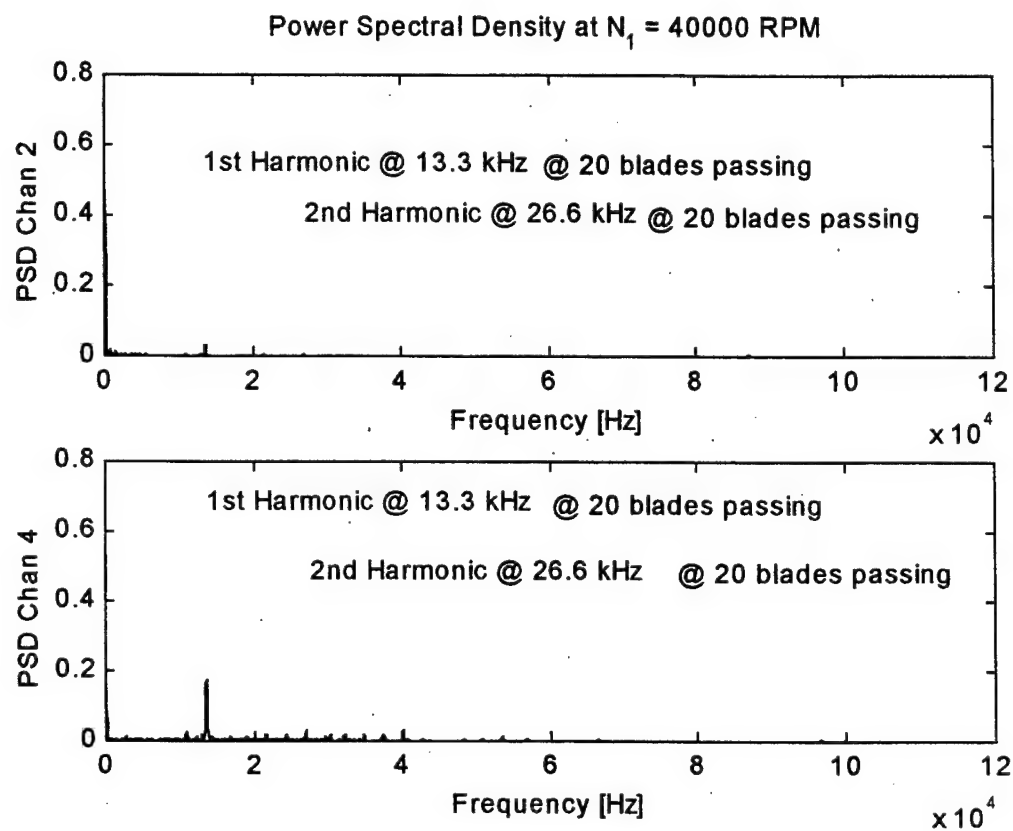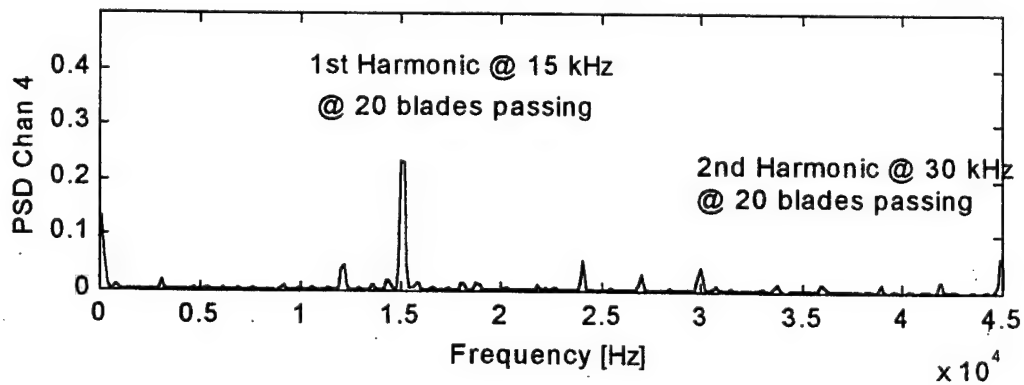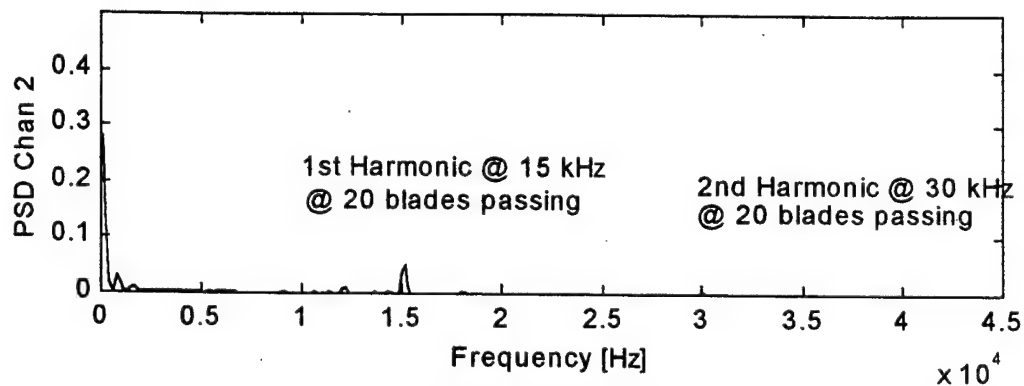
Power Spectral Density of Channels 2 and 4 at 40000 RPM

Power Spectral Density of Channels 1 and 3 at 45000 RPM

Power Spectral Density at N_1 = 45000 RPM

Power Spectral Density of Channels 2 and 4 at 45000 RPM

LIST OF REFERENCES

1. Muster, D., Stadelbauer, D. G., 1976, "Balancing of Rotating Machinery," Shock and Vibration Handbook Chapter 29, 2nd Edition, McGraw Hill.

2. Den Hartog, J. P., 1956, Mechanical Vibrations 4th Edition, McGraw Hill.

3. Williston, W. C., "Rotor Effect Driven By Fluid Forces From a Geometrically Imperfect Labyrinth Seal," Naval Postgraduate School, Monterey CA., Master's Thesis, Dec. 1993.

4. Millsaps, K. T., Williston, W. C., "Synchronous Rotor Vibration Driven By Fluid Forces from a Geometrically Imperfect Labyrinth Seal," 9S-GT-362, I.G.T.C., Houston TX., Jun 5-9, 1995.

5. Rains, D. A., "Tip Clearance Flows in Axial Flow Compressors and Pumps," California Institute of Technology, Hydrodynamics and Mechanical Laboratories, Report No. 5., Jun. 1954.

6. Lakshiminarayana, B., "Methods of Predicting the Tip Clearance Effects in Axial Flow Turbomachinery," ASME *Journal of Basic Engineering*, pp. 467-479, Sep. 1980.

7. Moyle, I. N., Walker, G. J., Shreeve, R. P., "Stator-Averaged, Rotor Blade-to-Blade Near Wall Flow in a Multistage Axial Compressor with Tip Clearance Variation," ASME *Journal of Turbomachinery*, Vol. 114, pp. 668-674, Jul. 1992.

8. Moyle, I. N., "An Experimental and Analytical Study of Tip Clearance Effects in Flow Axial Compressors," University of Tasmania, PhD, Dec. 1993.

9. McDougal, N. M., Cumpsty, N. A., Hynes, T. P., "Stall Inception in Axial Compressors," ASME *Journal of Turbomachinery*, Vol. 112, pp. 116-125, Jan. 1990

10. Firth, P. C., " The Effects of Compressor Rotor Tip Crops on Turboshaft Engine Performance," ASME, Journal of Engineering for Gas Turbines and Power, Vol. 116, pp. 184-189, Jan. 1994.

11. Moyle, I. N., "A Note on Efficiency Sensitivity to Tip Clearance Changes in Axial Flow Compressors," ASME *Journal of Turbomachinery*, Vol. 112, pp. 795-796, Oct. 1990.

12. Baghadi, S., "Modeling Tip Clearance Effects in Multistage Axial Compressors," ASME, *Journal of Turbomachinery*, Vol. 118, pp. 697-705, Oct. 1996.

13. Horlock, J. H., Greitzer E. M., "Non-uniform Flows in Axial Compressors due to Tip Clearance Variation," IMech, Proc. Instn. Mech Engrs., 1983, Vol 197C 173-178.

14. Graf, M. B., "Effects of Asymmetric Tip Clearances on Compressor Stability," Massachusetts Institute of Technology, Cambridge MA., M.Sc. Thesis, Jun. 1996.

15. Thomas H. J., "Unstable Natural Vibration of Turbine Rotors Induced by the Clearance Flow in Glands and Blading," Bull, de'l'A.I.M., Vol 71 No. 11/12, pp. 1039-1063, 1958.

16. Alford J., "Protecting Turbomachinery from Self-Excited Rotor Whirl," ASME Journal of Engineering for Power, pp. 333-334 Oct. 1965.

17. Urlichs K., "Clearance Flow-Generated Transverse Forces at the Rotors of Thermal Turbomachines," Disseration, Technical University of Munich. (English translation on NASA TM-77292, Oct. 1983), 1975.

18. Wohlrab R., "Experimental Determination of Gap-Flow Conditioned Force at Turbine Stages and Their Effect on Running Stability of Simple Rotors," Disseration, Technical University of Munich. (English translation on NASA TM-77293, Oct. 1983), 1975.

19. Vance J. M., "Instabilities in Turbomachinery," Proceeding of the 5th Annual Vibration Institute Seminar on Machinery Vibration Analysis, New Orleans LA., Apr. 1981.

20. Loose, D., "Experimental Investigation of Rotordynamic Isntabilities Caused by Rotor-Tip Excitation Forces," S.M. Thesis, Department of Aeronautics and Astronautics, M.I.T., 1992.

21. Song, S. J., Martinez-Sanches, M., "Rotordynamic Forces Due to Turbine Tip Leakage - Part I: Blade Effects," Transactions of ASME, 96-GT-364.

22. Song, S. J., Martinez-Sanches, M., "Rotordynamic Forces Due to Turbine Tip Leakage - Part II: Radius Scale Effects and Experimental Verification," Transactions of ASME, 96-GT-365.

23. Colding-Jorgenson, J., "Prediction of Rotor Dynamic Destablizing Forces in Axial Flow Compressors," ASME Journal of Fluids Engineering, Vol. 114, pp. 621-625, Dec. 1992.

24. Ehrich, F., "Rotor Whirl Forces Induced by the Tip Clearance Effect in Axial Flow Compressors," ASME Journal of Vibration and Acoustics, Vol. 115, pp. 509-515, Oct. 1993.

25. Vance J. M., Laudadio F. J., Experimental Measurement of Alford's Force in Axial Flow Turbomachinery," ASME Journal of Engineering for Gas Turbines and Power, Vol. 106, pp. 585-590, Jul. 1984.

26. Litang, Y., Jie, H., Qihan, L., Zigen, Z., Fuan, Z., "Blade Tip Destabilizing Force and Instability Analyses for Axial Rotors of Compressors," Beijing University of Aeronautics and Astronautics, Beijing, China, 100083, A95-40315, pp. 793-798.

27. Wisler, D., General Electric Aircraft Engines, Evandale OH., Personal communication via electronic mail, May-Jun.1997.

28. Storace, A., General Electric Aircraft Engines, Evandale OH.,Personal communication via electronic mail, May-Jun. 1997.

29. Eckerle, B. P., "Design and Component Integration of a T63-A-700 Gas Turbine Engine Test Facility," Master's Thesis, Naval Postgraduate School, Monterey CA, Sep. 1995.

30. Haas, D. W., "The Instrumentation Design and Control of a T63-A-700 Gas Turbine Engine", Master's Thesis, Naval Postgraduate School, Monterey CA, Jun. 1996.

31. Detriot Diesel Allison, "250 Series II Training Manual 10W12", Indianapolis, IN., Revision No. 3.

32. Detriot Diesel Allison, "Allison Gas Turbines, 250-C18 Series Installation Design," Indianapolis, IN., Publication No. 5W5, First Edition 2nd Revision, 15 January 1975.

33. Allison Division, "Detail Design Report T63-A-5A Turboshaft Engine," EDR 5900, Sep. 1968, Contract No. DAAJO1-67-C1289(3), Indianapolis, IN.

INITIAL DISTRIBUTION LIST

1. Defense Technical Information Center 2
    8725 John J. Kingman Road, Ste 0944
    Ft. Belvoir, Virginia 22060-6218

2. Dudley Knox Library 2
    Naval Postgraduate School
    411 Dyer Road
    Monterey, California 93943-5101

3. Department Chairman, Code-ME 1
    Department of Mechanical Engineering
    Naval Postgraduate School
    Monterey, California 93943-5101

4. Professor Knox T. Millsaps 3
    Mechanical Engineering Department, Code ME/MI
    Naval Postgraduate School
    Monterey, California 93943-5101

5. Naval/Mechanical Engineering Curriculum Officer...1
    Mechanical Engineering Department
    Naval Postgraduate School
    Monterey, California 93943-5101

6. U.S. Army Aviation and Missile Command 1
    Mr. Wess Cass
    ATTN AMSAM-MMC-VS-ECP.
    308 Crecy St
    Corpus Christi, Texas 78419

7. Naval Sea Systems Command 1
    Mr. Dan Groghan
    Director, Engines Division 03X3
    Washington D.C. 20362

8. Allison Engine Company 1
    Mr. Randall E. Yount
    P.O. Box 420
    Spd Code P39A
    Indianapolis, Indiana 46206-5748